

Electronic Supplementary Information for

# Organic structure and solid characteristics determine reactivity of phenolic compounds with synthetic and reclaimed manganese oxides

*Emma Leverich Trainer,<sup>1</sup> Matthew Ginder-Vogel,<sup>1,2</sup>† and Christina K. Remucal<sup>1,2</sup>\**

<sup>1</sup>Environmental Chemistry and Technology

University of Wisconsin - Madison

Madison, Wisconsin 53706

<sup>2</sup>Civil and Environmental Engineering

University of Wisconsin - Madison

Madison, Wisconsin 53706

**Contents (56 pages): Figures: S1-S13, Tables: S1-S19**

*Submitted to: Environmental Science: Water Research & Technology, September 26, 2019*

† Corresponding author address: 660 N. Park St., Madison, WI 53706;

e-mail: mgindervogel@wisc.edu; telephone: (608) 262-0768; fax: (608) 262-0454;

Twitter: @profmattgv.

\* Corresponding author address: 660 N. Park St., Madison, WI 53706;

e-mail: remucal@wisc.edu; telephone: (608) 262-1820; fax: (608) 262-0454; Twitter: @remucal.

## **Table of Contents**

<b>Section S1: Materials</b> .....	S3
<b>Section S2: Solid Characterization</b> .....	S6
<b>Section S3: Buffer Selection and Controls</b> .....	S9
<b>Section S4: Analytical Methods</b> .....	S10
<b>Section S5: Sorption Validation</b> .....	S16
<b>Section S6: Kinetic Modeling</b> .....	S18
<b>Section S7: Quantitative Structure Activity Relationship Data</b> .....	S21
<b>Section S8: QSAR Residuals and Validation</b> .....	S36
<b>References</b> .....	S54

## Section S1: Materials

All chemicals were commercially available and used as received. Details for all phenolic compounds are listed in **Table S1**; structures are displayed in **Table S2**.

Methanol (MeOH; HPLC grade), hydrochloric acid (HCl; Certified ACS Plus grade), sodium chloride (NaCl; Certified ACS grade), acetonitrile (HPLC grade), potassium permanganate (KMnO<sub>4</sub>; Certified ACS grade), and sodium hydroxide (NaOH; Certified ACS grade) were purchased from Fisher Scientific. Sulfuric acid (H<sub>2</sub>SO<sub>4</sub>; 95.0 – 98.0 %), nitric acid (HNO<sub>3</sub>; 70%), and L-ascorbic acid (BioXtra, ≥99%) were purchased from Sigma-Aldrich. Sodium oxalate (Na<sub>2</sub>C<sub>2</sub>O<sub>4</sub>; 99%) and sodium acetate trihydrate (ACS grade, 99 – 100.5%) were purchased from Alfa Aesar. Formic acid (HCOOH; Reagent ACS grade, 88%) was purchased from Aqua Solution, Inc. Manganese nitrate tetrahydrate (Mn(NO<sub>3</sub>)<sub>2</sub>•4H<sub>2</sub>O; analysis grade) was purchased from Acros Organics.

δ-MnO<sub>2</sub> was synthesized according to a modified Murray method.<sup>1</sup> By this method, Mn(NO<sub>3</sub>)<sub>2</sub> was added at a rate of 1 mL per minute into a solution of KMnO<sub>4</sub> and NaOH at molar ratios of 3:2:4 Mn<sup>II</sup>:Mn<sup>VII</sup>:OH<sup>-</sup> while stirring at 350 rpm. Following Mn(NO<sub>3</sub>)<sub>2</sub> addition, the solid suspension was covered and stirred for 18 hours at 22 ± 2 °C. The suspension was rinsed and washed by centrifugation at 2500 rpm for 15 minutes in ultrapure water, decreasing the suspension volume over six sequential rinse cycles. For the two final centrifuge rinses, the solids were resuspended in pH 5.5 10 mM acetate buffer solution. The density of the slurry was determined by drying 1 mL of the suspension at 60 °C in triplicate and calculating the amount of dry Mn per volume.

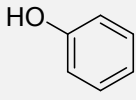
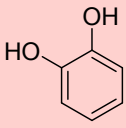
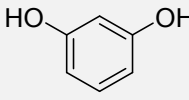
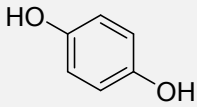
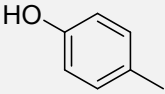
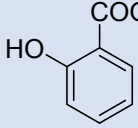
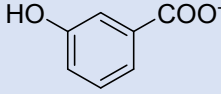
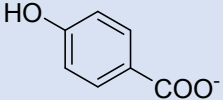
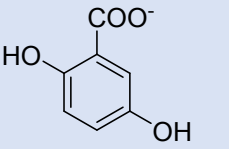
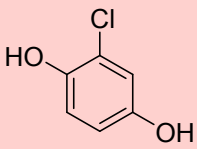
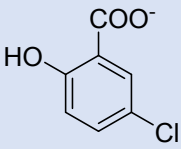
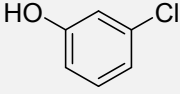
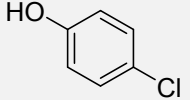
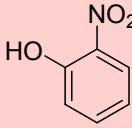
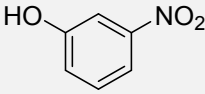
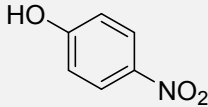
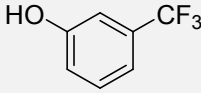
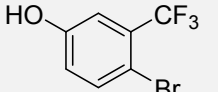
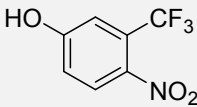
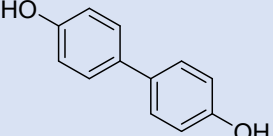
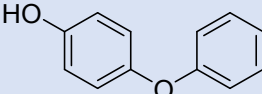
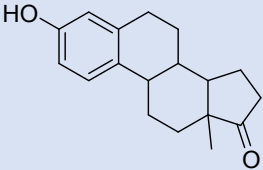
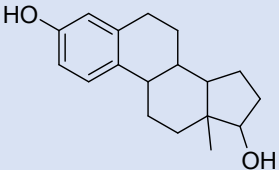
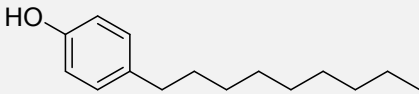
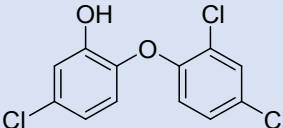
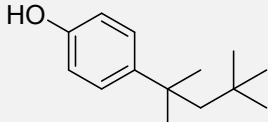
The acid mine drainage remediation (AMD) solids were collected and dried by Hedin Environmental from the Glasgow treatment site in Pennsylvania.<sup>2</sup> The filtered drinking water

treatment (DWT) solids were collected from Well 29 in Madison, WI. The DWT solids are the byproduct of a filter designed to remove aqueous manganese and iron that occur in the drinking water pumped at this well prior to disinfection and distribution. The solids were both rinsed with Milli-Q water (18.2 M $\Omega$ -cm) and equilibrated in 10 mM acetate buffer at 4 °C and adjusted to pH 5.5 until the pH remained stable.

**Table S1.** Sources and purity of phenols.

<b>Compound</b>	<b>Manufacturer</b>	<b>Purity</b>
phenol	Sigma-Aldrich	molecular biology
1,2-dihydroxybenzene (catechol)	Sigma-Aldrich	>99%
resorcinol (3-hydroxyphenol)	Alfa Aesar	99-100.5%
hydroquinone (4-hydroxyphenol)	Sigma-Aldrich	>99%
<i>p</i> -cresol (4-methylphenol)	Sigma-Aldrich	99%
salicylic acid (2-hydroxybenzoic acid)	Sigma-Aldrich	>99%
3-hydroxybenzoic acid	Aldrich	99%
4-hydroxybenzoic acid	Aldrich	99%
2,5-dihydroxybenzoic acid	Aldrich	98%
5-chlorohydroquinone	Acros Organics	90%
5-chlorosalicylic acid	Aldrich	98%
4-nitrocatechol	Alfa Aesar	98+%
2-chlorophenol	Aldrich	>99%
3-chlorophenol	Aldrich	98%
4-chlorophenol	Aldrich	>99%
2-nitrophenol	Aldrich	98%
3-nitrophenol	Sigma-Aldrich	99%
4-nitrophenol	Aldrich	>99%
3-trifluoromethylphenol	Aldrich	99%
4-bromo-3-trifluoromethylphenol	Alfa Aesar	98%
4-nitro-3-trifluoromethylphenol	Acros Organics	99%
4,4'-dihydroxybiphenyl	Aldrich	97%
4-phenoxyphenol	Sigma-Aldrich	99%
bisphenol A	Aldrich	>99%
estrone (E1)	Acros Organics	99+%
17 $\beta$ -estradiol (E2)	Sigma-Aldrich	>98%
4- <i>n</i> -nonylphenol	Alfa Aesar	98+%
triclosan	AccuStandard	N/A
4- <i>tert</i> -octylphenol	Sigma-Aldrich	97%

**Table S2.** Structures of phenols shown at pH 5.5. Gray cells are simple (i.e., *meta*- and *para*-substituted phenols), red cells are *ortho*-substituted phenols, and blue cells are complex phenols.

 phenol	 catechol	 resorcinol	 hydroquinone
 4-cresol	 2-hydroxybenzoate	 3-hydroxybenzoate	 4-hydroxybenzoate
 2,5-dihydroxybenzoate	 5-chlorohydroquinone	 5-chlorosalicylate	 4-nitrocatechol
 2-chlorophenol	 3-chlorophenol	 4-chlorophenol	
 2-nitrophenol	 3-nitrophenol	 4-nitrophenol	
 3-trifluoromethylphenol	 3-trifluoromethyl-4-bromophenol	 3-trifluoromethyl-4-nitrophenol	
 4,4'-dihydroxybiphenyl	 4-phenoxyphenol	 bisphenol A	
 estrone		 estradiol	
 4- <i>n</i> -nonylphenol	 triclosan	 4- <i>tert</i> -octylphenol	

## Section S2: Solid Characterization

The average manganese oxidation numbers (AMON) determined by X-ray absorption near-edge spectroscopy (XANES) and the oxalate titration method were compared for  $\delta$ -MnO<sub>2</sub>.<sup>3-5</sup> The oxalate titration determines the average oxidation state by dissolving the solid sample in excess sodium oxalate (0.5 g-Mn dissolved in 20 mL 100 mM Na<sub>2</sub>C<sub>2</sub>O<sub>4</sub> and 5 mL 6 M H<sub>2</sub>SO<sub>4</sub>), heating to 80 °C, and back titrating with 3 mM KMnO<sub>4</sub> (standardized against a Na<sub>2</sub>C<sub>2</sub>O<sub>4</sub> control sample prepared without Mn) until the solution begins to turn pink. The electron equivalents needed to fully oxidize the concentration of manganese in the sample are then converted to an average oxidation state based on the ratio of Mn<sup>III</sup>:Mn<sup>IV</sup>.<sup>5</sup> The results agreed well between the XANES and oxalate titration methods ( $3.8 \pm 0.2$ ) and are within the expected range for  $\delta$ -MnO<sub>2</sub>.<sup>1, 3, 6-11</sup> AMON values for the drinking water treatment and acid mine drainage remediation solids were also determined by XANES at the manganese edge ( $3.82 \pm 0.04$  and  $3.79 \pm 0.04$ , respectively). This method has a reported error of 0.04 valence units for solids ranging in valence from +3 to +4.<sup>3</sup>

Scanning electron microscopy (SEM; LEO 1530, Schottky-type field-emission electron source; **Figure S1**) was conducted to determine the general particle size, shape, and heterogeneity of these solids. The DWT solids are a heterogeneous mixture of particle size and shape, while the AMD solids have a more consistent particle size. SEM and transmission electron microscopy (TEM) images of  $\delta$ -MnO<sub>2</sub> show the consistent, amorphous shape and generally small particle size.<sup>1, 8, 12</sup> The  $\delta$ -MnO<sub>2</sub> used in this study is consistent with these previously published images.

The bulk elemental composition of the solids was determined by inductively coupled plasma-optical emission spectroscopy (ICP-OES; Perkin Elmer 4300; **Table S3**) of the material dissolved in 6 M HCl. From these analyses, the AMD solids contain inorganic impurities (e.g.,

Mg, Na) with trace amounts of other metals (e.g., Fe, Al, Ni). Because other redox active metals are only present in relatively low concentrations (**Table S3**), manganese is the primary redox active sorbent in this solid matrix. ICP-OES of the DWT solids indicate there are very few other trace metal species present (**Table S3**). ICP-OES was also used to determine the sodium content of  $\delta$ -MnO<sub>2</sub> dissolved in 6 M HCl ( $14.9 \pm 0.9$  % Na:Mn (mol:mol)).

The organic carbon content of each oxide was determined by weight loss on ignition. Pre-dried, finely ground solid (300 mg) was massed into a desiccated crucible. The samples were dried at 100° C for 16 hours then heated to 550° C for four hours to incinerate any organic carbon species.<sup>13</sup> The three solids had low organic carbon content as expected;  $\delta$ -MnO<sub>2</sub> had 0.7% organic carbon by weight, while the reclaimed drinking water treatment solids had 2.8% and the acid mine drainage remediation solids had 4.7% organic carbon by weight.

X-ray diffraction (XRD; Rigaku Rapid II, Mo K $\alpha$  source;  $\lambda = 0.7093$  Å; **Figure 2** in the manuscript) spectra also indicate differences between the solids. The pattern for  $\delta$ -MnO<sub>2</sub> is as expected for a poorly crystalline birnessite synthesized by the Murray method, with three characteristically broad peaks.<sup>1, 6, 7, 10, 12</sup> The DWT solids have a similarly low crystallinity, with even less defined peaks than  $\delta$ -MnO<sub>2</sub>, while XRD of the AMD solids confirms the presence of crystalline phases identified by SEM and EDS (**Figure 2**).

The pH of zero charge (pH<sub>pzc</sub>) was determined by rapid potentiometric titration performed with a Mettler Toledo G20 compact titrator and PNP sensor.<sup>14, 15</sup> To determine the pH at which the bulk surface is neutrally charged, 0.2 g of each solid were pre-equilibrated in solutions of 0.1 M, 0.01 M, and 0.001 M NaCl to control ionic strength for 24 hours. Following pre-equilibration, the solutions were adjusted to pH 11 with 1 M NaOH and allowed to shake overnight, then readjusted as needed to maintain a pH of 11. Blank solutions of each ionic strength were prepared

in the same manner. All solutions were titrated with 0.1 mL additions of 0.1 N H<sub>2</sub>SO<sub>4</sub> to a final pH of 0.5. The data was blank subtracted, normalized to the sample mass, and plotted versus pH. The pH<sub>pzc</sub> was identified as the intersect of the three ionic strength conditions for each solid. δ-MnO<sub>2</sub> and DWT data had multiple intersections; these values were averaged.

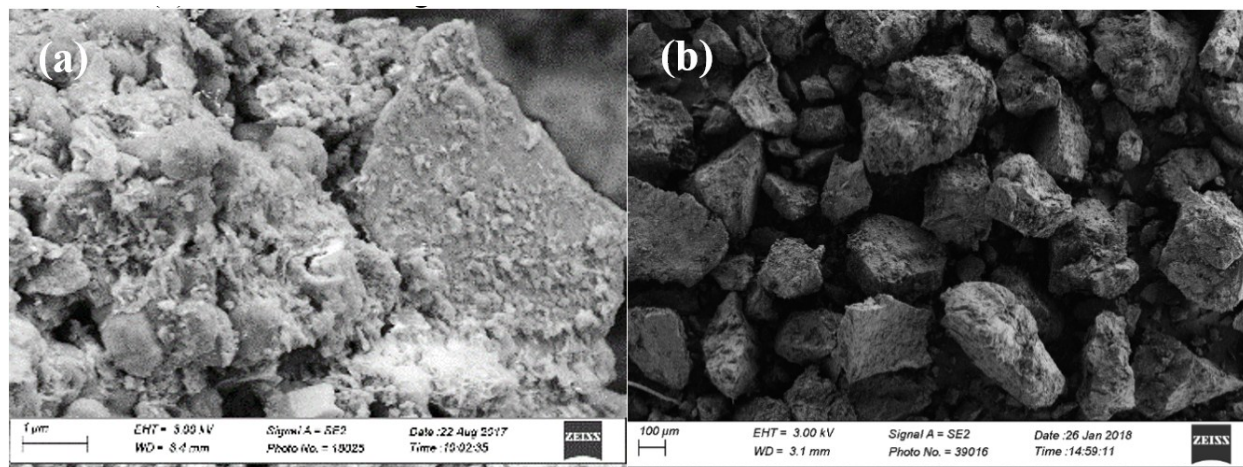


**Figure S1.** Scanning electron microscopy images of (a) drinking water treatment solids and (b) acid mine drainage remediation solids.

**Table S3.** Percent elemental composition (wt:wt) of metals and cations analyzed by ICP-OES for bulk solids extracted in 6 M HCl. N.D. indicates the element was below detection limits.

Solid	Mn	Fe	Zn	Al	Ni	Se	Ca	Mg	Na
δ-MnO <sub>2</sub>	63 ± 6	N.D.	N.D.	N.D.	N.D.	N.D.	N.D.	N.D.	15.0 ± 0.9
DWT	8.7 ± 0.8	43 ± 2	< 0.7	< 3	N.D.	0.8 ± 0.4	5.5 ± 0.1	0.4 ± 0.1	0.01 ± 0.02
AMD	42.8 ± 0.8	0.2 ± 0.2	0.98 ± 0.02	7.85 ± 0.01	0.61 ± 0.03	1 ± 7	-	0.63 ± 0.01	0.4 ± 0.8

### Section S3: Buffer Selection and Controls

**Sodium acetate buffer.** Sodium acetate buffer (pH 5.5) was selected because other buffers with buffering capacities in the range of pH 5 – 7 either interact with the manganese solids or, in the case of bicarbonate, do not adequately buffer these reactions under this experimental setup. Good's buffers (e.g., PIPES, MES) reduce manganese oxides and phosphate can strongly complex manganese sorption sites; previous studies using these buffers may be unreliable as these buffer interactions interfere with reported results.<sup>7, 10, 16-19</sup> In control experiments, 10 mM pH 6.5 bicarbonate buffer did not adequately buffer the system in non-purged batch reactors, with final reaction pH values ranging from 6.8 to 8.1 (data not shown). In contrast, reactors with 10 mM pH 5.5 sodium acetate buffer had an average final pH at  $5.59 \pm 0.06$  at the end of each reaction and showed no effects on the manganese structure or oxidation state.

**Control reactions of solids and phenols.** To test the effects that sodium acetate buffer may have on this system, control reactions were run for  $\delta$ -MnO<sub>2</sub>, DWT, and AMD solids in 10 mM pH 5.5 acetate buffer in the absence of phenolic compounds. AMON was determined by XANES for samples collected from the unreacted solids and after 10 days of equilibration in the buffer. There was no significant difference in AMON following the 10-day equilibrium period in pH 5.5 10 mM acetate buffer, indicating the sodium acetate buffer does not reduce these oxides over the maximum 10-day reaction period (**Table S4**).

**Table S4.** Average manganese oxidation number determined by XANES for manganese oxide starting materials and following 10-day equilibration in 10 mM pH 5.5 sodium acetate buffer without any organic reductants.

Manganese oxide	Initial AMON	Final AMON
$\delta$ -MnO <sub>2</sub>	$3.84 \pm 0.04$	$3.85 \pm 0.04$
DWT	$3.82 \pm 0.04$	$3.77 \pm 0.04$
AMD	$3.79 \pm 0.04$	$3.70 \pm 0.04$

## Section S4: Analytical Methods

**Phenol quantification.** An Agilent 1260 Infinity series high performance liquid chromatography instrument (HPLC; Agilent Technologies) was used to quantify the concentrations of all target phenolic compounds by an in-line diode array detector or fluorescence detector. Chromatography parameters are provided in **Table S5**. The aqueous mobile phase was 10% volume:volume (v:v) acetonitrile and 0.1% v:v formic acid adjusted to pH 2.5 in ultrapure water. Acetonitrile was the organic mobile phase. All phenolic compounds were analyzed using an EC-C18 column (Agilent Poroshell-120; 3.0 x 50 mm, 2.7  $\mu\text{m}$ ) with an injection volume of 20  $\mu\text{L}$ .

**Observed rate constants.** Experimental pseudo-first-order rate constants were determined for the quenched and filtered datasets collected for each phenol over the initial reaction period in triplicate (**Figure 1** in the manuscript; **Table S6**). These values are the pseudo-first-order rate constants of oxidation (quenched rate constant) and total removal (i.e., oxidation and sorption; filtered rate constants).

Hydroquinone is re-reduced by the ascorbic acid during quenching, preventing quenched rate determinations,<sup>20, 21</sup> while 2,5-dihydroxybenzoic acid is unreactive in the 10-day reaction period. The reaction mechanism and kinetic model results are shown, but these compounds were excluded from quantitative structure-activity modeling. Similarly, quenched rate constants for 4-nitrophenol and 3-trifluoromethyl-4-nitrophenol show loss, but the filtered rate constants are unavailable as the error was greater than the loss of these phenols.

**Table S5.** HPLC parameters for parent compound detection. The aqueous mobile phase was 10% v:v acetonitrile, 0.1% v:v formic acid at pH 2.5.

Compound	Aqueous mobile phase	Acetonitrile	Flow rate ( $\mu\text{L}/\text{min}$ )	Retention time (min)	Detection	
phenol	65%	35%	0.6	1	abs: 280 nm ref: 400 nm	
catechol	100%	0%		1.28		
resorcinol	40%	60%	1	0.4	Fluorescence: ex: 305 nm em: 290 nm	
hydroquinone	100%	0%	0.6	1.2	abs: 280 nm ref: 400 nm	
4-cresol	75%	25%		1.2	Fluorescence: ex: 305 nm em: 290 nm	
2-hydroxybenzoic acid	100%	0%		1.4	abs: 280 nm ref: 400 nm	
3-hydroxybenzoic acid				2.05		
4-hydroxybenzoic acid				1.5		
2,5-dihydroxybenzoic acid				1.8		
5-chlorohydroquinone				1.8		
5-chlorosalicylic acid				1.8		
4-nitrocatechol	100%	0%		2.5		
2-chlorophenol	75%	25%		3		
3-chlorophenol				3.5		
4-chlorophenol				3.5		
2-nitrophenol				3.5		
3-nitrophenol				2		
4-nitrophenol				1.5		
3-trifluoromethylphenol	65%	35%		2		
3-trifluoromethyl-4-bromophenol				3.5		
3-trifluoromethyl-4-nitrophenol				2		
4,4'-dihydroxybiphenyl	75%	25%		0.9		Fluorescence: ex: 305 nm em: 290 nm
bisphenol A	65%	35%		1		1.8
4-phenoxyphenol			2.8			
estrone			0.6	0.6		
17 $\beta$ -estradiol				3	Fluorescence: ex: 305 nm em: 290 nm	
4- <i>tert</i> -octylphenol	40%	60%	1	0.7	abs: 280 nm ref: 400 nm	
triclosan				1.45		
4- <i>n</i> -nonylphenol				3.1		

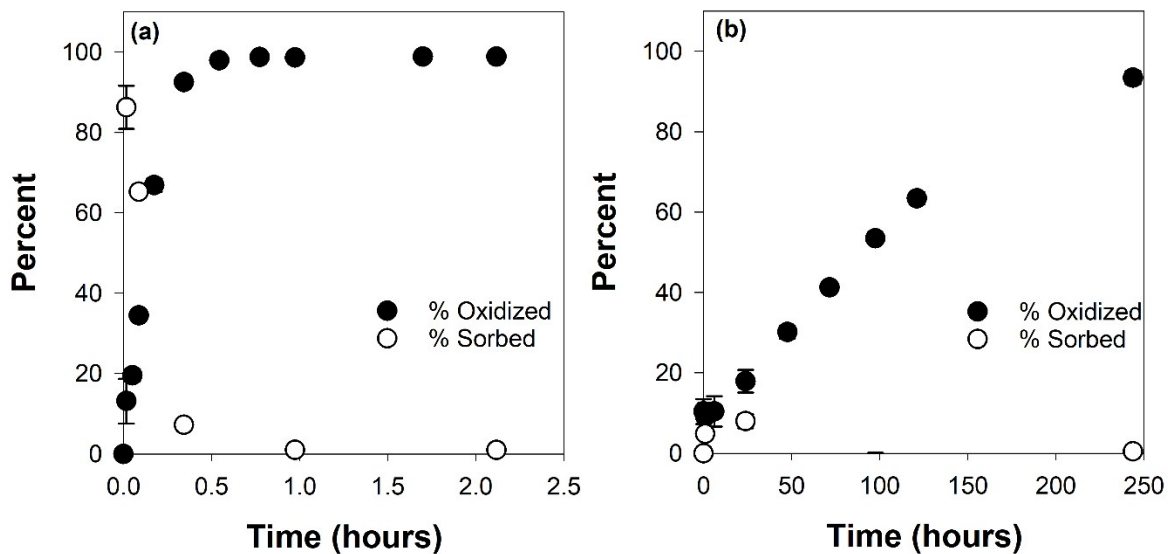


**Figure S2.** Percent sorption and loss for (a) triclosan and (b) 4,4'-dihydroxybiphenyl. Error bars indicate standard deviation of triplicate data.

**Table S6.** Quenched and filtered pseudo-first-order rate constants for 29 phenolic compounds reacted with  $\delta$ -MnO<sub>2</sub> and 15 phenols reacted with AMD and DWT reclaimed solids. The time for which the initial pseudo-first-order rate constants were determined and the observed rate-limiting step (RLS) for each reaction are included.

Compound	Quenched $k$ (hr <sup>-1</sup> )	Filtered $k$ (hr <sup>-1</sup> )	Analyzed reaction time (hr)	RLS
<i><math>\delta</math>-MnO<sub>2</sub></i>				
phenol	0.12 ± 0.03	0.20 ± 0.16	1.9	electron transfer
catechol	0.20 ± 0.07	0.18 ± 0.06	6.1	electron transfer
resorcinol	10.0 ± 0.6	25 ± 2	0.13	electron transfer
hydroquinone	-	35 ± 10	-	electron transfer
4-cresol	16 ± 11	47 ± 35	0.10	electron transfer
2-hydroxybenzoate	0.036 ± 0.009	0.006 ± 0.005	0.61	sorption
3-hydroxybenzoate	0.10 ± 0.04	1.2 ± 1.6	2.1	sorption
4-hydroxybenzoate	0.08 ± 0.02	0.9 ± 1.4	2.0	sorption
2,5-dihydroxybenzoate	0.079 ± 0.009	38.9 ± 0.5	14	electron transfer
5-chlorohydroquinone	0.033 ± 0.003	54.4 ± 0.5	48	electron transfer
5-chlorosalicylic acid	2.5 ± 2.3	0.21 ± 0.02	0.50	sorption
4-nitrocatechol	112 ± 6	355 ± 7	0.02	electron transfer
2-chlorophenol	1.2 ± 0.4	31 ± 18	0.56	electron transfer
3-chlorophenol	0.44 ± 0.09	0.51 ± 0.46	0.25	sorption
4-chlorophenol	2.8 ± 0.8	23 ± 16	0.13	electron transfer
2-nitrophenol	0.171 ± 0.002	0.11 ± 0.09	3.8	sorption
3-nitrophenol	0.01 ± 0.01	0.0003 ± 0.0007	3.8	sorption
4-nitrophenol	0.004 ± 0.002	-	6.1	sorption
3-trifluoromethylphenol	0.06 ± 0.03	0.08 ± 0.06	3.5	sorption
3-trifluoromethyl-4-bromophenol	0.11 ± 0.03	0.15 ± 0.13	3.4	sorption
3-trifluoromethyl-4-nitrophenol	0.001 ± 0.01	-	5.7	sorption
4,4'-dihydroxybiphenyl	0.009 ± 0.002	0.06 ± 0.07	182	sorption
4-phenoxyphenol	26 ± 1	82 ± 45	0.07	electron transfer
bisphenol A	8.5 ± 0.7	139 ± 84	0.20	electron transfer

Compound	Quenched $k$ (hr <sup>-1</sup> )	Filtered $k$ (hr <sup>-1</sup> )	Analyzed reaction time (hr)	RLS
<i>δ-MnO<sub>2</sub> continued</i>				
estrone	6.0 ± 0.5	53 ± 37	0.38	electron transfer
17β-estradiol	19 ± 10	90 ± 49	0.13	electron transfer
4- <i>n</i> -nonylphenol	1.5 ± 0.7	74 ± 10	0.26	electron transfer
triclosan	7.6 ± 0.2	126 ± 61	0.44	electron transfer
4- <i>tert</i> -octylphenol	149 ± 24	114 ± 33	0.04	sorption
<i>Drinking water treatment solids</i>				
phenol	0.02 ± 0.01	0.014 ± 0.007	25	sorption
resorcinol	0.08 ± 0.05	0.012 ± 0.007	9.6	sorption
4-cresol	0.12 ± 0.02	0.21 ± 0.16	4.5	electron transfer
4-nitrocatechol	0.8 ± 0.3	1.7 ± 1.1	1.6	electron transfer
2-chlorophenol	0.003 ± 0.001	0.0019 ± 0.0008	191	sorption
3-chlorophenol	0.003 ± 0.004	0.001 ± 0.003	67	electron transfer
4-chlorophenol	0.019 ± 0.005	0.03 ± 0.02	14	electron transfer
2-nitrophenol	0.001 ± 0.001	0.0003 ± 0.0007	87	sorption
3-nitrophenol	0.001 ± 0.002	0.003 ± 0.002	92	electron transfer
4,4'-dihydroxybiphenyl	0.026 ± 0.004	0.038 ± 0.003	107	electron transfer
4-phenoxyphenol	2.6 ± 2.9	11 ± 14	0.88	electron transfer
bisphenol A	0.10 ± 0.02	0.7 ± 0.4	2.6	electron transfer
estrone	0.09 ± 0.04	0.2 ± 0.1	7.1	electron transfer
triclosan	0.07 ± 0.10	0.03 ± 0.03	0.52	sorption
4- <i>tert</i> -octylphenol	0.54 ± 0.48	0.8 ± 1	33	electron transfer
<i>Acid mine drainage remediation solids</i>				
phenol	0.05 ± 0.03	0.001 ± 0.009	64	sorption
resorcinol	0.04 ± 0.04	0.06 ± 0.06	7.7	sorption
4-cresol	0.01 ± 0.01	0.01 ± 0.01	8.4	sorption

Compound	Quenched $k$ (hr <sup>-1</sup> )	Filtered $k$ (hr <sup>-1</sup> )	Analyzed reaction time (hr)	RLS
<i>Acid mine drainage remediation solids continued</i>				
4-nitrocatechol	1.1 ± 0.3	1.4 ± 0.5	1.5	electron transfer
2-chlorophenol	0.001 ± 0.001	0.002 ± 0.003	165	sorption
3-chlorophenol	0.001 ± 0.003	0.007 ± 0.015	32	electron transfer
4-chlorophenol	0.005 ± 0.004	0.8 ± 0.7	19	electron transfer
2-nitrophenol	0.0003 ± 0.002	0.003 ± 0.005	276	sorption
3-nitrophenol	-	-	-	electron transfer
4,4'-dihydroxybiphenyl	0.017 ± 0.004	0.018 ± 0.003	193	electron transfer
4-phenoxyphenol	0.09 ± 0.02	0.09 ± 0.02	7.9	sorption
bisphenol A	0.01 ± 0.03	0.008 ± 0.005	13	sorption
estrone	0.010 ± 0.008	0.02 ± 0.01	48	sorption
triclosan	0.03 ± 0.01	0.05 ± 0.03	0.14	sorption
4- <i>tert</i> -octylphenol	0.07 ± 0.03	0.2 ± 1.2	9.9	electron transfer

## Section S5: Sorption Validation

Previous literature identified the two potential rate limiting steps of phenol oxidation by manganese oxides as (1) the sorption process of the phenolate ion to the manganese reaction site, and (2) the first electron transfer between the sorbed phenolate and manganese center.<sup>7, 8</sup> If the reaction between the phenol and Mn oxide is sorption-limited, the sorption of the phenolate ion to the manganese surface site is the rate-limiting step of the reaction, indicating that after sorption occurs, the first electron transfer occurs relatively quickly. As a result, the phenol does not accumulate on the mineral surface and only low levels of the unreacted parent phenol are measured. The concentration of sorbed phenol was measured as the difference between the total phenol concentration (measured from the quenched aliquot) and the phenol concentration in the filtered aliquot (e.g., 4,4'-dihydroxybiphenyl in **Figure 1b** in the manuscript).

Alternatively, electron transfer-limited reactions are characterized by measurable phenol concentrations on the manganese surface. Because the rate of the first one-electron transfer is rate-limiting in this mechanism, the sorption of the phenol to the manganese surface is relatively fast. Therefore, phenol sorbs to the mineral surface and accumulates faster than electron transfer occurs. When this occurs, the quenched (i.e., total) phenol aliquot has a greater concentration than that of the filtered (i.e., dissolved) phenol aliquot taken at the same reaction timepoint. The difference represents the concentration of phenol sorbed to the manganese surface at that timepoint (e.g., triclosan in **Figure 1a**).

A maximum observed percent sorption of 10% was chosen to delineate electron transfer-limited versus sorption-limited mechanisms as a proxy for sorption rates compared to electron transfer rates. The maximum percent sorption is observed during the initial reaction period (in the first or second collected timepoint, **Figure S2**). This defined cutoff value was applied to the error

interval; compounds with high error for which one standard deviation from the reported percent sorption fell below the 10% cutoff were considered sorption-limited. Previous studies examining mechanistic differences between organic compounds<sup>8, 21-23</sup> or synthetic manganese oxides<sup>24</sup> do not outline a standard method for mechanism determination based on kinetic data.

We chose this operationally defined 10% cutoff based on observed trends in the data, as most phenols fell well above or below this cutoff amount, and a theoretical cutoff of 0% measured sorption does not account for instrumental and sampling error. Of the 27 phenols determined as sorption-limited (<10% sorption) with any solid oxidant, only two had greater than 5% sorption, with 7-8% observed sorption (4,4'-dihydroxybiphenyl reacted with  $\delta$ -MnO<sub>2</sub> and resorcinol reacted with DWT). On the other side of the defined 10% value, only 1 of the 22 phenols defined to be electron transfer-limited (3-nitrophenol reacted with DWT) had sorption values between 10-17%, at  $13 \pm 2\%$ . The results of kinetic modeling (**Section S6**) and rate constant trends in QSARs support the choice of a 10% maximum percent sorption cutoff for mechanism determination. The mechanism determined using the kinetic model agreed with experimental results using the 10% maximum sorption cutoff for 23 of 29 phenols reacted with  $\delta$ -MnO<sub>2</sub>. At a 5% cutoff, as explored above, only 19 of the 29 phenols would be predicted correctly.

## Section S6: Kinetic Modeling

We used the kinetic model developed by Zhang et al.<sup>22</sup> to test whether the oxidation mechanism-dependent modeled rate constants agree with the mechanisms determined by the measured sorption for reactions between  $\delta$ -MnO<sub>2</sub> and a suite of 29 phenols. This model fits the experimental time data to theoretical equations for electron transfer-limited (**Equation S1**) and sorption-limited mechanisms (**Equation S2**) by least squares regression.

$$C = (C_0 - S_{rxn}) + S_{rxn}e^{-k't} \quad \text{Equation S1}$$

$$C = \frac{S_{rxn} - C_0}{\frac{S_{rxn}}{C_0} e^{k''(S_{rxn} - C_0)t} - 1} \quad \text{Equation S2}$$

$$S_{rxn} = C_0 - C_e \quad \text{Equation S3}$$

$k'$  and  $k''$  are the calculated first- and second-order rate constants, respectively.  $C_0$  and  $C_e$  are the initial and equilibrium concentrations of the phenol,  $t$  is time, and  $S_{rxn}$  is the number of available surface sites on the solid. This value may be either fit to the data as a second variable or calculated as the difference between the initial and steady state concentrations of the compound (**Equation S3**). The latter was used here. After determining  $k''$  (units of M<sup>-1</sup> time<sup>-1</sup>), the value was multiplied by the initial concentration ( $C_0$ ; in M) to find the pseudo-first-order rate constant for this reaction mechanism (i.e.,  $k''*C_0$ ).

The values of the two theoretical pseudo-first-order rate constants,  $k'$  and  $k''*C_0$ , were compared using R<sup>2</sup> and root mean square error (RMSE) values for the fit of the modeled rate constant equation to the experimental loss data (**Figure S3**). The modeled rate constant giving the higher R<sup>2</sup> fit to the experimental loss data was selected as the modeled mechanism (e.g.,  $k'$ , the electron transfer-limited rate constant, when  $k'$  gave a higher R<sup>2</sup> fit). The values for  $k'$ ,  $k''$ ,  $k''*C_0$ , R<sup>2</sup> fits, and the determined mechanistic rate-limiting step are given in **Table S7**.

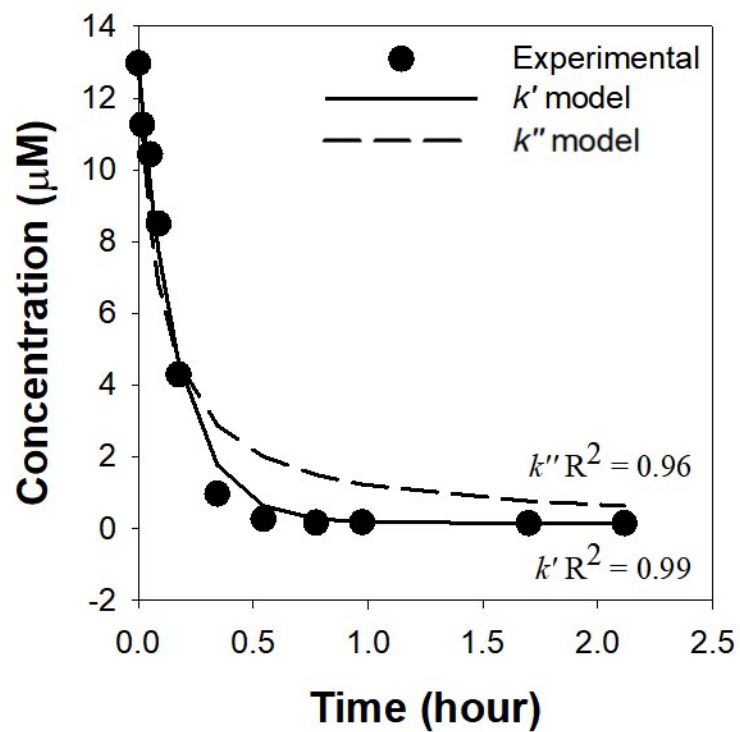


**Figure S3.** Experimental and modeled concentrations of triclosan versus time. The kinetic model fit for  $k'$  and  $k''$  determination is shown.

**Table S7.** Modeled  $k'$  and  $k''$ , respective  $R^2$  values, and pseudo-first-order  $k''*C_0$  values for 29 phenols reacted with  $\delta$ -MnO<sub>2</sub>.

<b>Compound</b>	<b><math>k'</math> (hr<sup>-1</sup>)</b>	<b><math>k' R^2</math></b>	<b><math>k''</math> (M<sup>-1</sup> hr<sup>-1</sup>)</b>	<b><math>k'' R^2</math></b>	<b><math>k''*C_0</math> (hr<sup>-1</sup>)</b>	<b>Model rate-limiting step</b>
phenol	0.87	0.994	0.08	0.991	0.97	electron transfer
catechol	0.22	0.99	0.03	0.95	0.32	electron transfer
resorcinol	11.4	0.999	2.51	0.98	18.8	electron transfer
hydroquinone	0.05	0.87	1.94	0.60	17.5	electron transfer
4-cresol	11.7	0.98	2.11	0.999	21.1	sorption
2-hydroxybenzoate	0.14	0.988	0.01	0.990	0.12	sorption
3-hydroxybenzoate	0.13	0.98	0.02	0.99	0.15	sorption
4-hydroxybenzoate	0.11	0.993	0.01	0.998	0.13	sorption
2,5-dihydroxybenzoate	0.11	0.99	0.01	0.96	0.16	electron transfer
5-chlorohydroquinone	0.12	0.89	0.02	0.88	0.17	electron transfer
5-chlorosalicylic acid	34.3	0.962	3.05	0.963	37.7	sorption
4-nitrocatechol	109.3	0.9997	23.1	0.98	220.6	electron transfer
2-chlorophenol	1.09	0.995	0.18	0.997	1.93	sorption
3-chlorophenol	0.63	0.996	0.10	0.997	0.85	sorption
4-chlorophenol	2.47	0.998	0.48	0.994	4.48	electron transfer
2-nitrophenol	0.47	0.998	0.06	0.997	0.48	electron transfer
3-nitrophenol	0.01	0.429	0.001	0.430	0.01	sorption
4-nitrophenol	0.01	0.687	0.001	0.690	0.01	sorption
3-trifluoromethylphenol	0.28	0.985	0.04	0.988	0.33	sorption
3-trifluoromethyl-4-bromophenol	0.29	0.995	0.04	0.996	0.37	sorption
3-trifluoromethyl-4-nitrophenol	0.04	0.995	0.004	0.996	0.04	sorption
4,4'-dihydroxybiphenyl	0.01	0.97	0.001	0.92	0.01	electron transfer
4-phenoxyphenol	25.6	0.999	5.32	0.97	47.7	electron transfer
bisphenol A	7.47	0.98	1.23	0.94	10.6	electron transfer
estrone	7.96	0.990	1.22	0.988	14.2	electron transfer
17 $\beta$ -estradiol	23.8	0.976	64.1	0.975	44.7	electron transfer
4- <i>n</i> -nonylphenol	2.78	0.960	21.2	0.964	3.27	sorption
triclosan	6.02	0.99	0.81	0.96	10.6	electron transfer
4- <i>tert</i> -octylphenol	158.63	0.9998	95.45	0.9999	1010	sorption

## Section S7: Quantitative Structure Activity Relationship Data

Descriptors for quantitative structure activity relationships (QSARs) were calculated using methods adapted from recent studies on organic compound oxidation.<sup>25-30</sup> In particular, the density functional theory modeling used in this study is based on the basis set, cross correlation, and solvation model comparisons and methods from Salter-Blanc et al.<sup>27</sup> The NWChem ESML API was used to model the specific QSAR descriptors energy of the highest occupied molecular orbital ( $E_{\text{HOMO}}$ ) and oxidation energy of the first electron ( $E_{\text{ox}}$ ). This resource was chosen as it represents the most user-friendly and widely available platform for calculating these specific molecular descriptors, and thus is a valuable tool to assess for the development of QSARs that rely on the availability of these calculations.  $E_{\text{HOMO}}$  was determined for the parent phenol or phenolate compound at pH 5.5, and values were used as given in the output.<sup>30</sup>  $E_{\text{ox}}$  values were determined for the half reaction of the loss of the first electron from the parent phenolate ion.<sup>26, 27, 30</sup> This modeled reaction output gives the  $\Delta G_{\text{rxn(aq)}}$  in units of  $\text{kcal mol}^{-1}$ , which was converted to an oxidation potential ( $E_{\text{ox}}$ ) via the Nernst equation, including a factor to convert to units of volts versus standard hydrogen electrode (V vs. SHE).<sup>26, 27, 30-32</sup>

$$E_{\text{ox}} = \frac{-G_{\text{rxn(aq)}}}{23.061} + 4.28 \quad \text{Equation S4}$$

After  $E_{\text{ox}}$  values were calculated from the Nernst equation, they were standardized to values reported by Pavitt et al.<sup>26</sup> by linear regression for compounds included in both studies ( $n = 15$ ; **Figure S4**). The resulting linear equation was applied to phenols in this study for which  $E_{\text{ox}}$  values are available (23 phenols) to give  $E_{\text{ox,corr.}}$  values.<sup>30</sup> QSAR plots and validation measurements for literature data (**Figure 6** in the manuscript; **Figure S5**) use  $E_{\text{ox}}$  values rather than  $E_{\text{ox,corr.}}$  to facilitate comparison. Descriptor values for all literature data were determined for this study using the same methods as described for the new experimental data to ensure consistency.

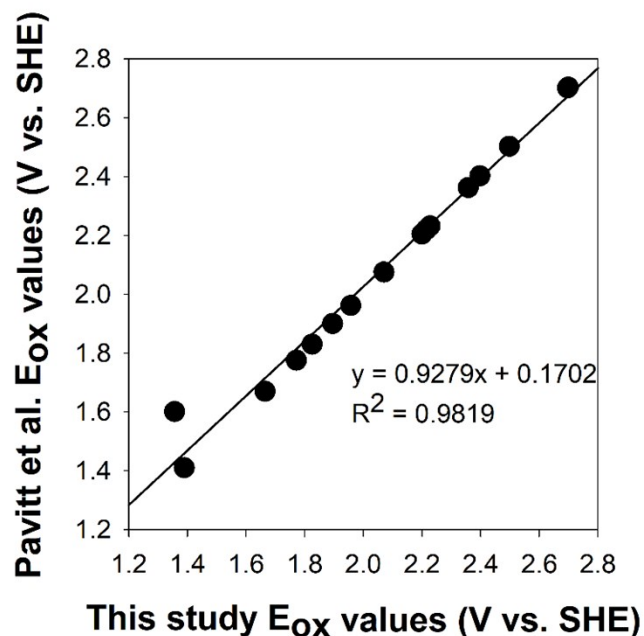


**Figure S4.**  $E_{\text{ox}}$  values versus oxidation potentials reported by Pavitt et al.<sup>26</sup> for phenolic compounds ( $n = 15$ ) calculated using the M06-2x theory. The linear regression shown was used to calculate  $E_{\text{ox,corr}}$  values.

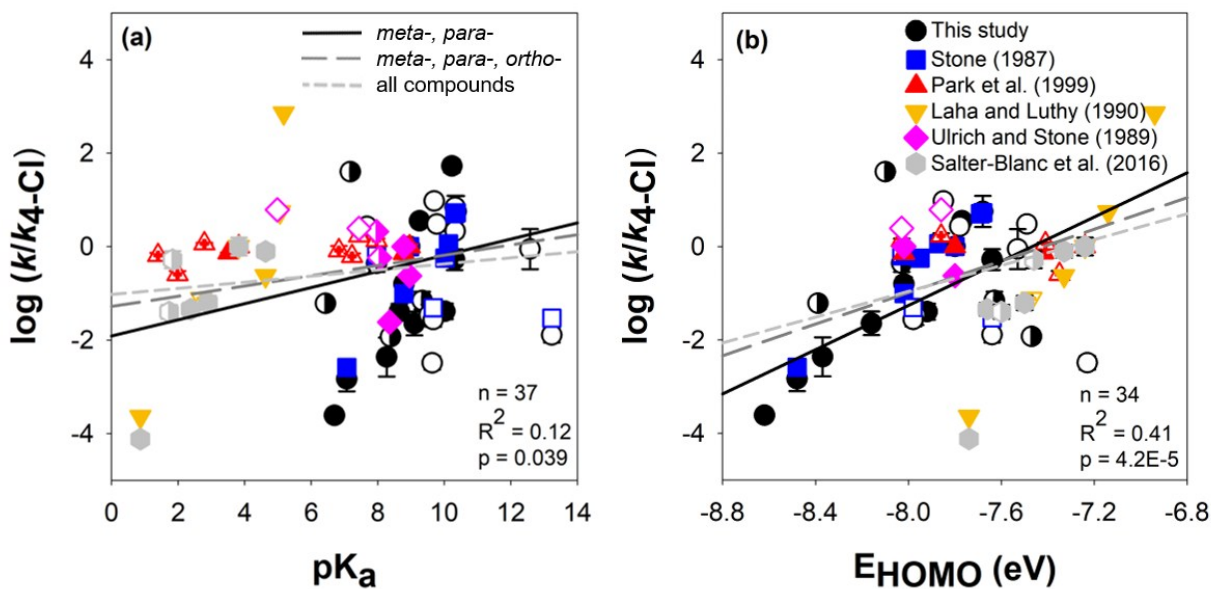


**Figure S5.** QSAR plots of normalized pseudo-first-order rate constants from literature<sup>8, 9, 27, 32, 33</sup> and  $\delta$ - $\text{MnO}_2$  reactions in this study versus (a)  $\text{pK}_a$  values of the speciated (e.g., phenol versus phenolate) compounds and (b) energy of the highest occupied molecular. Filled data points indicate *meta*- or *para*-substitution, *ortho*-substituted compounds are partially filled, and complex compounds are indicated by hollow points. Error bars indicate the standard deviation of triplicate measurements. Given regression values are for the simple *meta*- and *para*-compounds; regressions values for all lines are given in **Table S10**.

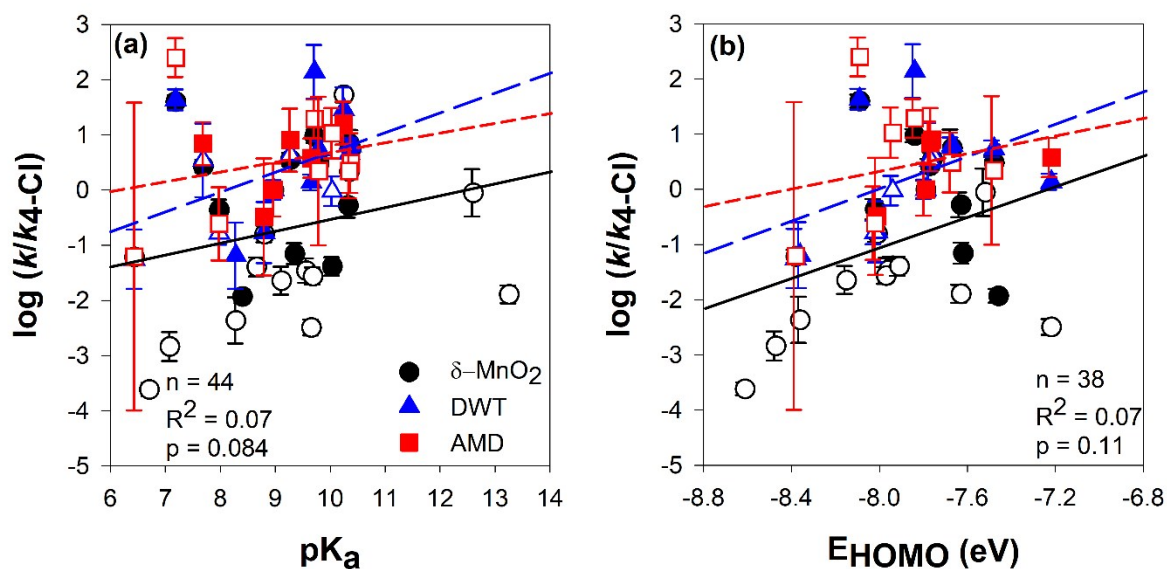


**Figure S6.** Quantitative structure-activity relationships for 15 phenols reacted with drinking water treatment and acid mine drainage remediation reclaimed solids and 29 phenols reacted with  $\delta$ -MnO<sub>2</sub>, all normalized to 15 mg-Mn L<sup>-1</sup>. Plots show the log of the average observed quenched rate constant normalized to the rate constant of 4-chlorophenol versus (a) first phenolic  $pK_a$  and (b) energy of the highest occupied molecular orbital. Error bars indicate the standard deviation of triplicate measurements. Filled data points indicate electron transfer-limited mechanisms and hollow data points indicate sorption-limited reaction mechanism. Lines indicate regression fits for all 15 phenols reacted with each manganese oxide; regressions values are given in **Table S11**.

**Table S8.** Calculated phenol descriptor data including QSAR Hammett constants,<sup>34-36</sup> predicted pK<sub>a</sub> values,<sup>37</sup> E<sub>HOMO</sub>, and E<sub>ox,corr.</sub>,<sup>38</sup> as well as the pK<sub>a</sub> corrected distribution ratio for the compound in octanol versus water (log D<sub>ow</sub>),<sup>37</sup> and partitioning coefficients for soil organic carbon to water (log K<sub>oc</sub>) and octanol to water (log K<sub>ow</sub>).<sup>39</sup>

	log (k/k <sub>4-Cl</sub> ) with δ-MnO <sub>2</sub>	Hammett constant	pK <sub>a</sub>	E <sub>HOMO</sub> (eV)	E <sub>ox,corr.</sub> (V vs. SHE)	log D <sub>ow</sub> at pH 5.5	log K <sub>oc</sub> (L/kg)	log K <sub>ow</sub>
<i>Simple (meta-, para-) compounds</i>								
phenol	-1.38 ± 0.17	0	10.02	-7.95	1.92	1.67	2.27	1.46
resorcinol	0.55 ± 0.12	0.1	9.26	-7.77	1.86	1.37	2.38	0.93
hydroquinone	-	-0.36	9.68	-7.41	1.44	1.37	2.38	0.59
4-cresol	0.75 ± 0.33	-0.16	10.36	-7.68	1.70	2.18	2.48	1.94
3-chlorophenol	-0.80 ± 0.15	0.37	8.79	-8.02	2.24	2.27	2.48	2.5
4-chlorophenol	0.00 ± 0.17	0.22	8.96	-7.8	1.80	2.27	2.48	2.39
3-nitrophenol	-2.36 ± 0.42	0.73	8.27	-8.37	2.36	1.61	2.46	2
4-nitrophenol	-2.84 ± 0.26	1.25	7.07	-8.48	2.50	1.60	2.46	1.91
3-trifluoromethylphenol	-1.64 ± 0.25	0.44	9.1	-8.16	2.06	2.55	3.10	2.95
3-trifluoromethyl-4-bromophenol	-1.39 ± 0.17	0.67	8.65	-7.92	2.51	3.32	-	-
3-trifluoromethyl-4-nitrophenol	-3.61 ± 0.12	1.69	6.7	-8.62	2.70	2.46	3.31	2.87
4- <i>n</i> -nonylphenol	-0.28 ± 0.22	-0.16	10.31	-7.64	1.83	5.74	4.58	5.76
4- <i>tert</i> -octylphenol	1.73 ± 0.14	-0.1	10.23	-	-	4.69	4.00	4.93
<i>ortho-substituted compounds</i>								
catechol	-1.15 ± 0.19	-	9.34	-7.63	1.41	1.37	2.39	0.88
5-chlorohydroquinone	-1.93 ± 0.12	-	8.39	-7.47	-	1.97	2.60	1.4
4-nitrocatechol	1.60 ± 0.12	-	7.18	-8.1	2.12	1.30	2.58	1.66
2-chlorophenol	-0.36 ± 0.18	-	7.97	-8.03	1.98	2.27	2.50	2.15
2-nitrophenol	-1.21 ± 0.12	-	6.43	-8.39	2.40	1.59	2.47	1.79

Compound	$\log(k/k_{4-Cl})$ with $\delta\text{-MnO}_2$	Hammett constant	$\text{pK}_a$	$E_{\text{HOMO}}$ (eV)	$E_{\text{ox,corr.}}$ (V vs. SHE)	$\log D_{\text{ow}}$ at pH 5.5	$\log K_{\text{oc}}$ (L/kg)	$\log K_{\text{ow}}$
<i>Complex compounds</i>								
2-hydroxybenzoic acid	$-1.89 \pm 0.16$	-	13.23	-7.64	2.69	-0.72	1.34	2.26
3-hydroxybenzoic acid	$-1.46 \pm 0.22$	-	9.55	-7.97	2.21	-0.38	1.33	1.5
4-hydroxybenzoic acid	$-1.56 \pm 0.15$	-	9.67	-7.98	2.69	0.13	1.33	1.58
2,5-dihydroxybenzoic acid	-	-	10.02	-7.25	1.71	-1.23	1.45	1.74
5-chlorosalicylic acid	$-0.05 \pm 0.43$	-	12.58	-7.53	2.21	-0.28	1.54	3.09
4,4'-dihydroxybiphenyl	$-2.49 \pm 0.14$	0.01	9.64	-7.23	1.85	3.01	3.93	2.8
4-phenoxyphenol	$0.97 \pm 0.12$	-	9.7	-7.85	1.53	3.17	3.39	3.35
bisphenol A	$0.48 \pm 0.12$	-	9.78	-7.49	2.23	4.05	4.58	3.32
estrone	$0.33 \pm 0.12$	-	10.33	-	-	4.31	4.38	3.13
17 $\beta$ -estradiol	$0.84 \pm 0.25$	-	10.33	-	-	3.75	4.19	4.01
triclosan	$0.43 \pm 0.12$	-	7.68	-7.78	2.09	4.98	4.37	4.76

**Table S9.** Regression statistics for QSAR descriptors versus normalized observed initial rate constants of 29 phenols reacted with  $\delta$ -MnO<sub>2</sub> (**Figure 4** in the manuscript) calculated for 95% confidence interval. Gray values indicate  $p < 0.005$ ; bold values are  $p < 0.05$ .

Substitution	Hammett Constant			pK <sub>a</sub>			E <sub>HOMO</sub>			E <sub>ox,corr.</sub>		
	n	R <sup>2</sup>	p	n	R <sup>2</sup>	p	n	R <sup>2</sup>	p	n	R <sup>2</sup>	p
Simple	12	0.76	2.2E-4	12	0.69	8.5E-4	11	0.89	1.3E-5	11	0.77	3.9E-4
Simple + <i>ortho</i>	15	0.60	6.8E-4	17	0.55	6.9E-4	16	0.29	0.032	15	0.37	0.016
All substituents	16	0.46	4.2E-3	27	0.16	0.040	24	0.13	0.084	23	0.29	8.2E-3

**Table S10.** Regression statistics for QSAR descriptors versus normalized literature rate constants and reactions of 29 phenols with  $\delta$ -MnO<sub>2</sub> (**Figure 6** in the manuscript; **Figure S5**) calculated for 95% confidence interval. Literature data available in **Table S12**. Gray values indicate  $p < 0.005$ ; bold values are  $p < 0.05$ .

Substitution	Hammett Constant			pK <sub>a</sub>			pK <sub>a</sub> phenols			pK <sub>a</sub> anilines			E <sub>HOMO</sub>			E <sub>ox,corr.</sub>		
	n	R <sup>2</sup>	p	n	R <sup>2</sup>	p	n	R <sup>2</sup>	p	n	R <sup>2</sup>	p	n	R <sup>2</sup>	p	n	R <sup>2</sup>	p
Simple	37	0.74	1.2E-11	37	0.12	0.039	25	0.68	3.7E-7	12	0.84	2.4E-5	34	0.41	4.2E-5	34	0.35	2.3E-4
Simple + <i>ortho</i>	53	0.25	1.3E-4	54	0.06	0.069	37	0.16	0.014	17	0.57	4.3E-4	48	0.23	5.9E-4	47	0.21	1.1E-3
All substituents	55	0.16	2.5E-3	69	0.02	0.21	51	0.00	0.75	18	0.57	2.7E-4	60	0.14	2.9E-3	59	0.17	1.2E-3

**Table S11.** Regression statistics for QSAR descriptors versus normalized observed initial rate constants of 15 phenols reacted with  $\delta$ -MnO<sub>2</sub>, drinking water treatment solids, and acid mine drainage remediation solids (**Figure 5** in the manuscript; **Figure S6**) calculated for 95% confidence interval. Gray values indicate  $p < 0.005$ ; bold values are  $p < 0.05$ .

Solid phases	Hammett Constant			pK <sub>a</sub>			E <sub>HOMO</sub>			E <sub>ox,corr.</sub>		
	n	R <sup>2</sup>	p	n	R <sup>2</sup>	p	n	R <sup>2</sup>	p	n	R <sup>2</sup>	p
$\delta$ -MnO <sub>2</sub>	10	0.18	2.2E-1	15	0.03	5.6E-1	13	0.01	7.3E-1	13	0.13	2.3E-1
DWT	<b>10</b>	<b>0.75</b>	<b>1.2E-3</b>	15	0.19	1.1E-1	13	0.02	1.2E-1	<b>13</b>	<b>0.40</b>	<b>2.0E-2</b>
AMD	<b>9</b>	<b>0.81</b>	<b>1.0E-3</b>	14	0.06	4.0E-1	12	0.06	4.4E-1	12	0.16	2.0E-1
All solids	<b>29</b>	<b>0.41</b>	<b>2.0E-4</b>	44	0.07	8.3E-2	38	0.07	1.1E-1	<b>38</b>	<b>0.20</b>	<b>4.5E-3</b>

**Table S12.** Literature data sources and reported reaction conditions.

Compound	Reported loss	Reported loss method	log ( $k/k_{4-Cl}$ )	buffer	[Organic] ( $\mu$ M)	[Mn]	Ionic strength	AMON; Surface Area	Mn synthesis method
<i>Park, 1999</i> <sup>33</sup>									
2-chlorophenol	62 ± 0.6	Quenched; % loss in 24 hr	0.14 ± 0.04	pH 5.6; 200 mM acetate	300	0.5 g/L	Not reported	Not reported	McKenzie
3-chlorophenol	32.8 ± 5.6		-0.14 ± 0.08						
4-chlorophenol	45.4 ± 3.8		0 ± 0.05						
2,4-dichlorophenol	77.6 ± 6.4		0.23 ± 0.05						
2,5-dichlorophenol	28.4 ± 3.1		-0.20 ± 0.06						
2,4,5-trichlorophenol	37.6 ± 7.9		-.08 ± 0.10						
2-chloroaniline	99.6 ± 0.8		0.07 ± 0.02						
3-chloroaniline	63.7 ± 0.5		-0.1288 ± 0.0001						
4-chloroaniline	85.7 ± 4.2		0 ± 0.03						
2,4-dichloroaniline	22 ± 3.4		-0.59 ± 0.07						
2,4,5-trichloroaniline	56.1 ± 6		-0.18 ± 0.05						
<i>Laha and Luthy, 1990</i> <sup>32</sup>									
aniline	10.4	Filtered; second-order rate constant ( $M^{-1} \text{ min}^{-1}$ )	-0.626	pH 4 or 4.4; acetate	2500	5 mM	0.1 M NaNO <sub>3</sub>	Not reported	Murray
4-chloroaniline	44		0		5000	5 mM			
4-methoxyaniline	32000		2.86		62	33 $\mu$ M			
4-methylaniline	240		0.737		2000	2.5 mM			
4-nitroaniline	0.01		-3.643		2000	5 mM			
4-aminobenzoic acid	3.44		-1.107		5000	5 mM			

Compound	Reported	Reported	log ( $k/k_{4-Cl}$ )	buffer	[Organic]	[Mn]	Ionic	AMON;	Manganese
----------	----------	----------	----------------------	--------	-----------	------	-------	-------	-----------

	loss	loss method			( $\mu\text{M}$ )		strength	Surface Area	synthesis method
<i>Ulrich and Stone, 1989<sup>9</sup></i>									
2-chlorophenol	0.11	Filtered, then quenched; first-order rate constant ( $\text{min}^{-1}$ )	-0.237	pH 4.2 or 4.84 2.5 mM acetate	150	0.16 mM	50 mM NaCl	3.93; S.A. not reported	Boiling, purged, 1.98 mM $\text{Mn}(\text{ClO}_4)_2$ + 10.3 mM NaOH + 10.4 mM NaOCl
3-chlorophenol	0.018		-1.023		140				
4-chlorophenol	0.19		0						
2,4-dichlorophenol	0.4		0.323		110				
3,4-dichlorophenol	0.045		-0.626		120				
3,5-dichlorophenol	0.0046		-1.616		120				
2,4,6-trichlorophenol	1.17		0.789		140				
pentachlorophenol	0.47		0.393		11				
<i>Stone, 1987<sup>8</sup></i>									
phenol	2.22E-07	Filtered; zero-order rate constant ( $\text{M min}^{-1}$ )	-0.244	pH 4.4; 1 mM acetate	100	48 $\mu\text{M}$	50 mM NaCl	3.81; 25 $\text{m}^2 \text{g}^{-1}$	MnSO <sub>4</sub> + 2 mM NaMnO <sub>4</sub> in pH 6.6, 50 mM phosphate buffer
2-hydroxybenzoate	1.15E-08		-1.529						
4-hydroxybenzoate	1.93E-08		-1.304						
2-chlorophenol	2.48E-07		-0.195						
3-chlorophenol	3.84E-08		-1.006						
4-chlorophenol	3.89E-07		0						
4-nitrophenol	1.00E-09		-2.590						
3-methylphenol	4.48E-07		0.061						
4-methylphenol	2.06E-06		0.724						
4-ethylphenol	1.97E-06		0.705						

Compound	Reported loss	Reported loss	$\log(k/k_{4\text{-Cl}})$	buffer	[Organic] ( $\mu\text{M}$ )	[Mn]	Ionic strength	AMON; Surface	Manganese synthesis
----------	---------------	---------------	---------------------------	--------	-----------------------------	------	----------------	---------------	---------------------

		method						Area	method
<i>Salter-Blanc et al., 2016<sup>27</sup></i>									
aniline	0.0216 ± 0.0012	Filtered or quenched; first-order rate constant (sec <sup>-1</sup> )	-0.10 ± 0.14	pH 6; 10 mM bicarbonate	10	Not reported	0.1 M NaCl	Not reported	Murray and Villalobos
4-chloroaniline	0.0272 ± 0.0085		0 ± 0.2						
3-nitroaniline	0.00125 ± 5.69e-5		-1.3 ± 0.1						
4-nitroaniline	2.06E-06		-4.121						
4-methyl-3-nitroaniline	0.0017 ± 0.0003		-1.2 ± 0.2						
2-methoxy-5-nitroaniline	0.0143 ± 0.0041		-0.28 ± 0.18						
2-methyl-5-nitroaniline	0.00109 ± 1.55e-4		-1.4 ± 0.1						

**Table S13.** Literature QSAR descriptors. Log ( $k/k_{4-Cl}$ ) values calculated based on reported loss rates (**Table S12**). Hammett constants, pK<sub>a</sub> values, E<sub>HOMO</sub> and E<sub>ox</sub> values determined in this study.

Compound	Category	log ( $k/k_{4Cl}$ )	Hammett constant	pK <sub>a</sub>	E <sub>HOMO</sub> (eV)	E <sub>ox</sub> (V vs. SHE)
<i>Park, 1999</i> <sup>33</sup>						
2-chlorophenol	<i>ortho</i>	0.14 ± 0.04	0.68	7.97	-8.03	1.96
3-chlorophenol	simple	-0.14 ± 0.08	0.37	8.79	-8.02	2.23
4-chlorophenol	simple	0 ± 0.05	0.22	8.96	-7.8	1.77
2,4-dichlorophenol	<i>ortho</i>	0.23 ± 0.05	0.9	7.44	-7.86	2.08
2,5-dichlorophenol	<i>ortho</i>	-0.20 ± 0.06	1.05	7.23	-	-
2,4,5-trichlorophenol	<i>ortho</i>	-0.08 ± 0.10	1.27	6.83	-	-
2-chloroaniline	<i>ortho</i>	0.07 ± 0.02	0.67	2.79	-7.41	1.38
3-chloroaniline	simple	-0.1288 ± 0.0001	0.37	3.52	-7.42	1.37
4-chloroaniline	simple	0 ± 0.03	0.22	3.83	-7.24	1.26
2,4-dichloroaniline	<i>ortho</i>	-0.59 ± 0.07	0.89	1.98	-7.35	1.50
2,4,5-trichloroaniline	<i>ortho</i>	-0.18 ± 0.05	1.26	1.4	-	-
<i>Laha and Luthy, 1990</i> <sup>32</sup>						
aniline	simple	-0.63	0	4.63	-7.33	1.21
4-chloroaniline	simple	0	0.22	3.83	-7.24	1.26
4-methoxyaniline	simple	2.86	0.12	5.17	-6.94	0.83
4-methylaniline	simple	0.74	-0.16	5.06	-7.14	1.01
4-nitroaniline	simple	-3.64	1.25	0.87	-7.74	1.71
4-aminobenzoate	complex	-1.11	-	2.69	-7.47	1.75
<i>Ulrich and Stone, 1989</i> <sup>9</sup>						
2-chlorophenol	<i>ortho</i>	-0.24	0.68	7.97	-8.03	1.96
3-chlorophenol	simple	-1.02	0.37	8.79	-8.02	2.23
4-chlorophenol	simple	0	0.22	8.96	-7.8	1.77

Compound	Category	Log ( $k/k_{4cl}$ )	Hammett constant	pK <sub>a</sub>	E <sub>HOMO</sub> (eV)	E <sub>ox</sub> (V vs. SHE)
<i>Ulrich and Stone, 1989<sup>9</sup> cont.</i>						
2,4-dichlorophenol	<i>ortho</i>	0.32	0.9	7.44	-7.86	2.08
3,4-dichlorophenol	simple	-0.63	0.59	8.36	-	-
3,5-dichlorophenol	simple	-1.62	0.74	8.06	-	-
2,4,6-trichlorophenol	<i>ortho</i>	0.79	1.58	5.99	-8.02	2.14
pentachlorophenol	complex	0.39	2.32	4.98	-	-
<i>Stone, 1987<sup>8</sup></i>						
phenol	simple	-0.24	0	10.02	-7.95	1.90
2-hydroxybenzoate	complex	-1.53	-	13.23	-7.64	1.37
4-hydroxybenzoate	complex	-1.3	-	9.67	-7.98	2.27
2-chlorophenol	<i>ortho</i>	-0.19	0.68	7.97	-8.03	1.96
3-chlorophenol	simple	-1.01	0.37	8.79	-8.02	2.23
4-chlorophenol	simple	0	0.22	8.96	-7.8	1.77
4-nitrophenol	simple	-2.59	1.25	7.07	-8.48	2.50
3-methylphenol	simple	0.06	-0.06	10.13	-7.87	1.90
4-methylphenol	simple	0.72	-0.16	10.36	-7.68	1.67
4-ethylphenol	simple	0.70	-0.15	10.32	-7.69	1.71
<i>Salter-Blanc et al., 2016<sup>27</sup></i>						
aniline	simple	-0.10 ± 0.14	0	4.63	-7.33	1.21
4-chloroaniline	simple	0 ± 0.2	0.22	3.83	-7.24	1.26
3-nitroaniline	simple	-1.3 ± 0.1	0.73	2.38	-7.66	1.58
4-nitroaniline	simple	-4.12	1.25	0.87	-7.74	1.71
4-methyl-3-nitroaniline	simple	-1.2 ± 0.2	0.57	2.90	-7.5	1.39
2-methoxy-5-nitroaniline	<i>ortho</i>	-0.28 ± 0.18	0.75	1.83	-7.46	1.38
2-methyl-5-nitroaniline	<i>ortho</i>	-1.4 ± 0.1	0.83	1.73	-7.60	1.52

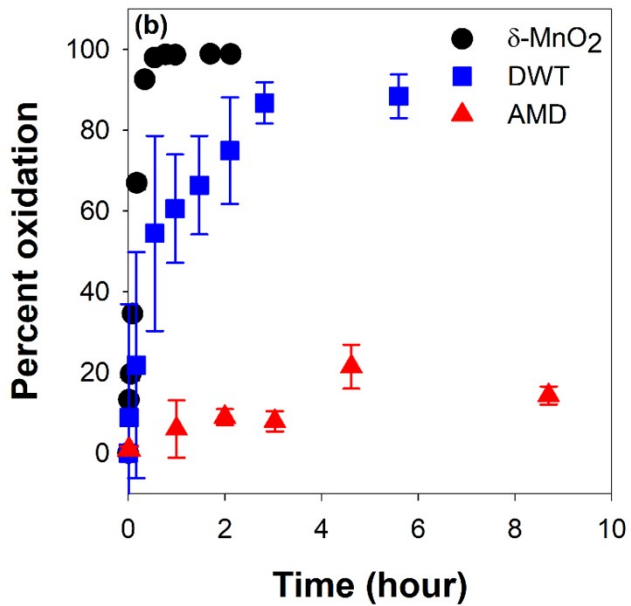
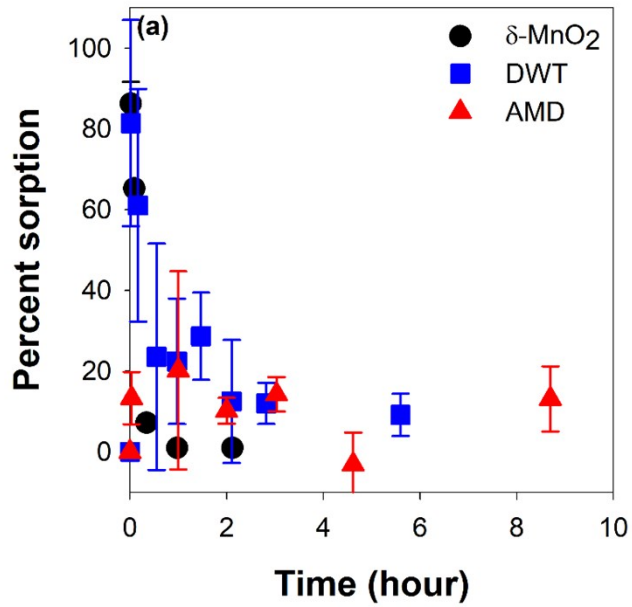


**Figure S7.** Percent of initial triclosan concentration (a) sorbed to solid surface and (b) oxidized over the first 10 hours of reaction with  $\delta$ -MnO<sub>2</sub>, DWT solids, and AMD solids. Error bars represent the standard deviation of triplicate measurements.

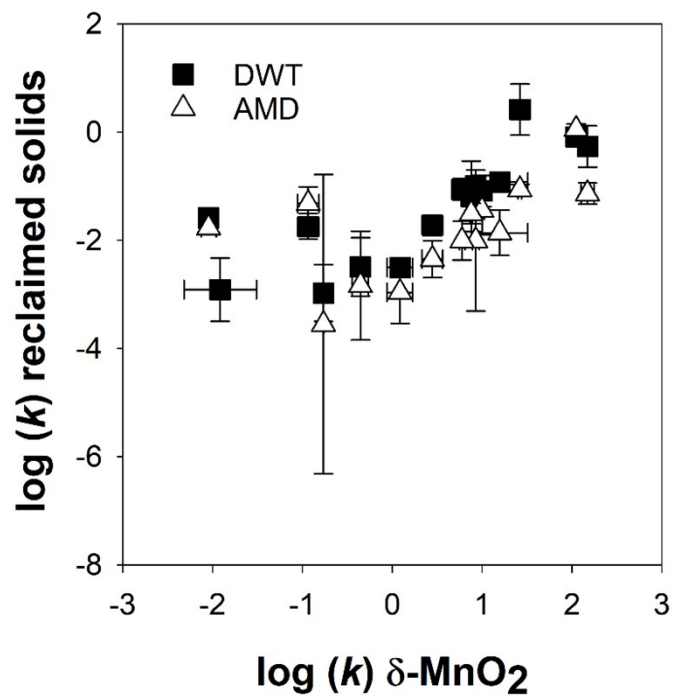


**Figure S8.** Comparison of  $\log k$  for DWT and AMD solids with  $\delta\text{-MnO}_2$  reacted with 15 phenols. Error bars indicate the standard deviation of triplicate measurements.

**Table S14.** Observed oxidation rate-limiting step for phenols reacted with  $\delta$ -MnO<sub>2</sub>, DWT, and AMD solids.

<b>Compound</b>	<b><math>\delta</math>-MnO<sub>2</sub></b>	<b>DWT</b>	<b>AMD</b>
phenol	electron transfer	sorption	sorption
resorcinol	electron transfer	sorption	sorption
estrone	electron transfer	electron transfer	sorption
4-cresol	electron transfer	electron transfer	sorption
4- <i>tert</i> -octylphenol	sorption	electron transfer	electron transfer
bisphenol A	electron transfer	electron transfer	sorption
4-phenoxyphenol	electron transfer	electron transfer	sorption
4-nitrocatechol	electron transfer	electron transfer	electron transfer
triclosan	electron transfer	sorption	sorption
2-chlorophenol	electron transfer	sorption	sorption
3-chlorophenol	sorption	electron transfer	electron transfer
4-chlorophenol	electron transfer	electron transfer	electron transfer
2-nitrophenol	sorption	sorption	sorption
3-nitrophenol	sorption	electron transfer	electron transfer
4,4'-dihydroxybiphenyl	sorption	electron transfer	electron transfer

## Section S8: QSAR Residuals and Validation

The residuals of each developed quantitative structure-activity relationships were analyzed to determine the normality of the data to the linear fit. Residuals were calculated from the data from this study (**Figures 4 and 5** in the manuscript) and literature rates (**Figure 6**) for the QSAR lines developed with only the simple *meta*- and *para*-substituted compounds, as well as the QSAR relationships developed with all plotted compounds to consider both the simplest and most all-encompassing linear relationships. In the case of the QSARs developed using the data from the three studied manganese oxides, the linear models including data from individual solids and all three solids combined were used for the simple and all-encompassing cases, respectively. From the linear QSAR relationships, we calculated predicted values of normalized  $\log(k/k_{4-Cl})$  from the QSAR descriptors (e.g., Hammett constants), then this predicted y term was subtracted from the experimental value to ascertain each residual value (**Tables S15 – S17**). Positive values indicate the experimental value was larger than the predicted (i.e., the model underpredicts the normalized rate constant) and negative values indicate the model overpredicted the observed rate constant terms.

The calculated residuals were plotted against the independent QSAR descriptor values to test for random distribution (**Figures S9 and S10**). If the developed linear model is a good fit for the data, the residuals should fall in a random manner around the x-axis across the range of the independent variable.<sup>40</sup> As some of the resulting plots show non-random behavior (i.e., linear or funnel-like trends) while in other the randomness is ambiguous, we also plotted the residuals against the probability of each residual. To do this, the residuals were ranked in ascending order and the rank of each residual (i) and the total sample size (N) were used to predict the probability, P, for that value.

$$P = \frac{i}{(N + 1)} \quad \text{Equation S5}$$

The resulting plots should lay along a clear line if the data is distributed normally. Bimodal, or 's' shaped, data trends indicate the residuals are not normally distributed. As a result, bimodal distributions suggest the data used to develop the linear model should be transformed to achieve a better fit, or that the relationship is better fit by another power of relationship.<sup>40</sup>

The predictive strength of the developed QSAR was also tested using external validation strategies. External validation separates data into test and training data sets. A training QSAR is built from the training data set and the linear regression from that data is used to predict reactivity values for the test set. The predicted and experimental values are compared statistically to determine the predictive strength of the overall QSAR. Typically, the independent variables of the QSAR are first internally validated to determine which predictive descriptors best correlate with reactivity; however, since we are interested in evaluating literature QSAR models, the same independent variables were used as in those studies.<sup>26, 27, 32, 41</sup>

To test the predictive strength of the QSARs included in this study, validation statistics were adopted from bioinformatics QSAR validation studies.<sup>42-45</sup>  $R^2$  is the common squared correlation coefficient determined between the predicted and experimental values for the test set.  $r_0^2$  is the squared correlation coefficient between predicted and experimental values with an intercept set to (0,0).  $r_m^2$ , calculated from  $R^2$  and  $r_0^2$  (**Equation S6**), is a value for external validation that is advantageous for small test sets. This value determines whether the range of predicted values falls near that of observed values. In **Table S18**, this value is accompanied by the equivalent measurements for reversed axes ( $r_m^{2'}$ ; i.e., predicted versus experimental values and experimental versus predicted values).

$R^2_{pred}$  is also an external validation comparing the test set predicted and experimental values, as well as the average training set dependent variable (i.e.,  $\log k/k_{4-Cl}$ ), as shown in **Equation S7**. The shown minimum value of 0.5 is less conservative, as some sources argue 0.6 is a better minimum value.<sup>44</sup>  $R^2_p$  (**Equation S8**) corrects for the differences between randomized and non-randomized test sets, to determine whether the other statistics are true indicators of the QSAR's robust nature, rather than chance.

$$r_m^2 = R^2(1 - \sqrt{R^2 - r_0^2}) \quad \text{Equation S6}$$

$$R_{pred}^2 = 1 - \frac{\sum_1^{test} (\log^{[rot]}(\frac{k}{k_{4-Cl}})_{exp} - \log^{[rot]}(\frac{k}{k_{4-Cl}})_{pred})^2}{\sum_1^{test} (\log^{[rot]}(\frac{k}{k_{4-Cl}})_{exp} - \log^{[rot]}(\frac{\bar{K}}{k_{4-Cl}})_{training})^2} \quad \text{Equation S7}$$

$$R_p^2 = R^2(1 - \sqrt{|R^2 - R_r^2|}) \quad \text{Equation S8}$$

The range of accepted values for comparing the experimental and predicted  $\log(k/k_{4-Cl})$  values for each defined test set based on the correlating training set are included in **Table S18** and summarized in Veerasamy et al.<sup>44</sup>

These validation measurements include 27 phenols reacted with  $\delta$ -MnO<sub>2</sub> in this study as well as all literature data analyzed in this study. The total maximum sample size was 69 points, excluding any phenols for which experimental  $\log(k/k_{4-Cl})$  values are not available (hydroquinone and 2,5-dihydroxybenzoate). The total sample size is smaller in conditions for which QSAR descriptors are not available for all included compounds (e.g., a lack of tabulated Hammett constants). The overall data set is small for QSAR development but demonstrates whether the current state of the literature allows for accurate reactivity predictions for phenolic contaminants as previous studies have suggested. The data set is also large enough to support trends outlined in

the manuscript by clarifying the relationship between compound structure and QSAR predictability.

To determine the ability of commonly studied *meta*- and *para*-substituted phenols to predict the behavior of *ortho*- and complex compounds, the data was dividing into test and training sets for all four QSAR parameters (i.e., Hammett constants,  $pK_a$ ,  $E_{HOMO}$ , and  $E_{ox}$ ) based on substituent placement. This non-random division of data was chosen to investigate whether the linear relationships developed based on simple, well-studied phenols can accurately predict the pseudo-first-order rate constants for *ortho*-substituted or complex phenolic contaminants of environmental concern. The QSARs developed for four independent descriptors were also probed by separating test and training sets based on this study ( $\delta$ -MnO<sub>2</sub> data) versus literature data (**Table S18**) and by using  $\delta$ -MnO<sub>2</sub> data to predict  $\log(k/k_{4-Cl})$  values for reclaimed solids (**Table S19**). This division was chosen to scrutinize whether normalized, pseudo-first-order  $\log k$  values follow the same trend across reaction conditions. Specifically, we tested whether a historic data set collected across studies with varying reaction conditions is able to predict the normalized trends in a specific study and whether a synthetic manganese oxide data set (e.g.,  $\delta$ -MnO<sub>2</sub>) can predict normalized  $\log k$  values for reclaimed solids with varying solid composition and characteristics. Both overall data sets (i.e., synthetic manganese oxides with data from this study and literature, and this study's data for  $\delta$ -MnO<sub>2</sub> and reclaimed solids) were also tested using randomized training and test sets (about 70% and 30% of the overall data sets, respectively; one randomization per QSAR descriptor).

To be validated, multiple measures should fall within the respective acceptable ranges for the QSAR in question. Where the analyzed QSAR relationships do fall within the accepted range of a validation measurement (e.g.,  $R^2_{pred}$ ,  $r_m^2$ ), it is only for one validation test variable, indicating

the regression is useful under the conditions tested by that variable (e.g., linearity, non-random correlation) but the QSARs are not predictive across all analyzed validity conditions. Only the literature training set,  $\delta$ -MnO<sub>2</sub> test set division of data fell within the accepted ranges for multiple measures ( $R^2_{\text{pred}}$  and  $p$ ). This indicates the included literature data was potentially predictive towards the normalized pseudo-first-order rate constants of the compounds included in this study, but only with necessarily structurally selective Hammett constants as the independent descriptor. That scenario is also not necessarily applicable for other compounds or reaction (or environmental) conditions, even using Hammett constants as a descriptor, as the division of data was non-random.

**Table S15.** Residual values calculated against the *meta*- and *para*-substituted and all compound QSARs developed with data from this study. QSAR linear regressions provided in **Table S9**.

	Simple substituents				All substituents			
	$\Sigma\sigma$	pK <sub>a</sub>	E <sub>HOMO</sub>	E <sub>ox,corr.</sub>	$\Sigma\sigma$	pK <sub>a</sub>	E <sub>HOMO</sub>	E <sub>ox,corr.</sub>
phenol	-1.1	-0.9	-0.4	-0.9	-1.4	-1.6	-0.5	-1.0
catechol		-0.4	-0.6	-1.7		-0.6	-1.6	-2.6
resorcinol	1.0	1.3	1.3	0.9	0.7	1.2	0.7	0.7
hydroquinone								
4-cresol	0.8	1.1	1.4	0.8	0.3	0.2	0.5	0.4
2-hydroxybenzoate		-2.6	-1.3	0.08		-5.6	-2.3	1.3
3-hydroxybenzoate		-0.8	-0.5	-0.4		-1.1	-0.5	-0.002
4-hydroxybenzoate		-1	-0.5	0.4		-1.4	-0.6	1.6
2,5-dihydroxybenzoate								
5-chlorohydroquinone		-0.9	-1.6			-0.4	-3.0	
5-chlorosalicylic acid		-0.5	0.3	1.0		-3.0	-0.9	1.4
4-nitrocatechol		3.1	2.8	2.5		4.5	3.0	2.7
2-chlorophenol		0.8	0.7	0.2		1.7	0.8	0.3
3-chlorophenol	0.1	0.1	0.3	0.3	0.02	0.3	0.3	0.8
4-chlorophenol	0.7	0.8	0.8	0.2	0.5	1.0	0.2	0.001
2-nitrophenol		0.5	0.4	0.2		2.5	1.4	0.9
3-nitrophenol	-0.8	-1.3	-0.8	-1.0	-0.6	-0.7	0.1	-0.4
4-nitrophenol	-0.4	-1.3	-1.1	-1.2	0.07	0.2	0.1	-0.4
3-trifluoromethylphenol	-0.6	-0.9	-0.4	-0.9	-0.7	-0.8	0.03	-0.7
3-trifluoromethyl-4-bromophenol	0.06	-0.4	-0.5	0.2	0.1	-0.1	-0.7	1.1
3-trifluoromethyl-4-nitrophenol	-0.4	-2	-1.7	-1.6	0.3	-0.2	-0.1	-0.4
4,4'-dihydroxybiphenyl	-2.2	-1.9	-2.5	-2.2	-2.5	-2.3	-4.5	-2.3
4-phenoxyphenol		1.6	1.8	0.7		1.1	1.4	0.004
bisphenol A		1.0	0.8	1.5		0.6	-0.5	2.0
estrone		0.7				-0.2		
17 $\beta$ -estradiol		1.2				0.3		
4- <i>n</i> -nonylphenol	-0.3	0.08	0.3	-0.01	-0.7	-0.8	-0.7	-0.2
triclosan		2.8	0.6	1.5		1.7	1.2	1.2
4- <i>tert</i> -octylphenol	1.4	1.3			1.8	2.1		

**Table S16.** Residual values calculated against the *meta*- and *para*-substituted and all compound QSARs developed with data from this study and compiled from literature. QSAR linear regressions provided in **Table S10**.

	Simple substituents				All substituents			
	$\Sigma\sigma$	pK <sub>a</sub>	E <sub>HOMO</sub>	E <sub>ox</sub>	$\Sigma\sigma$	pK <sub>a</sub>	E <sub>HOMO</sub>	E <sub>ox</sub>
<i>This study</i>								
phenol	-1.7	-1.2	-0.2	-0.5	-1.3	-1.0	-0.5	-0.7
catechol		-1.5	-0.8	-1.3		-1.5	-0.7	-1.1
resorcinol	0.5	0.9	1.3	1.3	0.7	1.0	1.2	1.1
hydroquinone								
4-cresol	0.002	0.9	1.3	1.2	0.7	1.1	1.3	1.1
2-hydroxybenzoate		-2.3	-1.5	0.5		-1.7	-1.4	-0.3
3-hydroxybenzoate		-1.2	-0.3	0.02		-1.1	-0.5	-0.4
4-hydroxybenzoate		-1.3	-0.3	0.9		-1.2	-0.6	0.07
2,5-dihydroxybenzoate								
5-chlorohydroquinone	-1.4	2.3	-1.9		-1.6	2.2	-1.7	
5-chlorosalicylic acid		-0.3	0.1	1.4		0.2	0.3	1.0
4-nitrocatechol		0.2	3.1	2.9		0.1	2.7	2.5
2-chlorophenol	1.1	-0.4	1.0	0.7	0.3	-0.6	0.6	0.4
3-chlorophenol	-0.1	-0.4	0.5	0.7	-0.4	-0.4	0.2	0.3
4-chlorophenol	0.3	0.4	0.8	0.7	0.3	0.4	0.7	0.5
2-nitrophenol	1.7	1.4	1.0	0.6	0.01	1.1	0.3	0.05
3-nitrophenol	-0.7	-1.9	-0.2	-0.6	-1.6	-1.9	-0.9	-1.1
4-nitrophenol	0.2	-2.1	-0.4	-0.8	-1.6	-2.3	-1.2	-1.5
3-trifluoromethylphenol	-0.8	-1.3	-0.002	-0.5	-1.2	-1.2	-0.5	-0.8
3-trifluoromethyl-4-bromophenol	0.06	-1.0	-0.3	0.7	-0.7	-0.9	-0.5	0.01
3-trifluoromethyl-4-nitrophenol	0.5	-2.9	-0.9	-1.2	-2.0	-3.0	-1.8	-2.0
4,4'-dihydroxybiphenyl	-2.8	-2.2	-3.1	-1.7	-2.4	-2.1	-2.6	-1.9
4-phenoxyphenol		1.2	1.9	1.1		1.4	1.7	1.1
bisphenol A		0.7	0.5	2.0		0.9	0.7	1.5
estrone		0.5				0.7		
17 $\beta$ -estradiol		1.0				1.2		
4- <i>n</i> -nonylphenol	-1.0	-0.2	0.1	0.5	-0.4	0.07	0.2	0.3
triclosan		1.0	1.1	1.7		1.0	1.1	1.3
4- <i>tert</i> -octylphenol	1.1	1.9			1.7	2.1		
<i>Park, 1999<sup>30</sup></i>								
2-chlorophenol	1.6	0.6	1.5	1.2	0.8	0.5	1.1	0.9
3-chlorophenol	0.5	0.3	1.2	1.4	0.3	0.3	0.8	0.9
4-chlorophenol	0.3	0.4	0.8	0.7	0.3	0.4	0.7	0.5
2,4-dichlorophenol	2.3	0.5	1.2	1.5	1.1	0.3	1.0	1.1
	<b>Simple substituents</b>				<b>All substituents</b>			

	$\Sigma\sigma$	$pK_a$	$E_{HOMO}$	$E_{ox}$	$\Sigma\sigma$	$pK_a$	$E_{HOMO}$	$E_{ox}$
<i>Park, 1999<sup>30</sup> continued</i>								
2,5-dichlorophenol	2.3	1.5			0.8	0.7		
2,4,5-trichlorophenol	3.0	0.9			1.2	0.8		
2-chloroaniline	1.5	-0.9	-0.07	0.009	0.8	-0.7	0.2	0.1
3-chloroaniline	0.5	1.2	-0.2	-0.2	0.3	0.7	0.02	-0.1
4-chloroaniline	0.3	1.3	-0.5	-0.3	0.3	0.8	-0.1	-0.1
2,4-dichloroaniline	1.4	1.5	-0.9	-0.4	0.3	0.9	-0.5	-0.4
2,4,5-trichloroaniline	2.8	1.0			1.1	0.3		
<i>Laha and Luthy, 1990<sup>32</sup></i>								
aniline	-1.0	0.5	-1.0	-1.0	-0.6	0.08	-0.6	-0.8
4-chloroaniline	0.3	1.3	-0.5	-0.3	0.3	0.8	-0.1	-0.1
4-methoxyaniline	2.9	3.9	1.6	1.8	3.0	3.5	2.3	2.2
4-methylaniline	-0.01	1.8	-0.04	0.001	0.6	1.4	0.5	0.3
4-nitroaniline	-0.7	-1.9	-3.0	-3.1	-2.4	-2.7	-3.0	-3.2
4-aminobenzoic acid		0.3	-1.1	-0.5		-0.3	-0.9	-0.6
<i>Ulrich and Stone, 1989<sup>9</sup></i>								
2-chlorophenol	1.2	0.9	1.1	0.8	0.5	0.9	0.8	0.5
3-chlorophenol	-0.4	-0.6	0.3	0.5	-0.6	-0.6	-0.04	0.04
4-chlorophenol	0.3	0.4	0.8	0.7	0.3	0.4	0.7	0.5
2,4-dichlorophenol	2.4	0.3	1.3	1.6	1.2	0.3	1.1	1.2
3,4-dichlorophenol	0.6	-0.2			-0.01	-0.1		
3,5-dichlorophenol	0.02	-1.1			-0.8	-1.1		
2,4,6-trichlorophenol	4.7	1.7	2.1	2.2	2.3	1.4	1.8	1.7
pentachlorophenol	6.2	0.3			2.6	0.3		
<i>Stone, 1987<sup>8</sup></i>								
phenol	-0.6	-0.06	0.9	0.7	-0.2	0.1	0.6	0.4
2-hydroxybenzoate		-1.9	-1.1	-1.6		-1.4	-1.1	-1.5
4-hydroxybenzoate		-1.1	-0.09	0.3		-0.9	-0.4	-0.2
2-chlorophenol	1.3	1.3	1.1	0.8	0.5	0.6	0.8	0.5
3-chlorophenol	-0.4	-0.6	0.3	0.5	-0.6	-0.6	-0.02	0.05
4-chlorophenol	0.3	0.4	0.8	0.7	0.3	0.4	0.7	0.5
4-nitrophenol	0.4	-1.9	-0.2	-0.6	-1.4	-2.0	-1.0	-1.2
3-methylphenol	-0.4	0.2	1.0	1.0	0.06	0.4	0.8	0.7
4-methylphenol	-0.03	0.8	1.2	1.2	0.6	1.1	1.2	1.1
4-ethylphenol	-0.02	0.8	1.2	1.3	0.6	1.1	1.2	1.1
<i>Salter-Blanc et al., 2016<sup>27</sup></i>								
aniline	-0.4	1.0	-0.4	-0.5	-0.05	0.6	-0.07	-0.3
4-chloroaniline	0.3	1.3	-0.5	-0.3	0.3	0.8	-0.1	-0.1
	<b>Simple substituents</b>				<b>All substituents</b>			
	$\Sigma\sigma$	$pK_a$	$E_{HOMO}$	$E_{ox}$	$\Sigma\sigma$	$pK_a$	$E_{HOMO}$	$E_{ox}$

*Salter-Blanc et al., 2016<sup>27</sup> continued*

3-nitroaniline	0.3	0.2	-0.9	-1.0	-0.6	-0.5	-0.9	-1.1
4-nitroaniline	-1.1	-2.4	-3.5	-3.6	-2.9	-3.2	-3.5	-3.7
4-methyl-3-nitroaniline	-0.02	0.2	-1.1	-1.2	-0.6	-0.4	-0.9	-1.1
2-methoxy-5-nitroaniline	1.4	0.2	-0.3	-0.3	0.5	-0.5	-0.07	-0.2
2-methyl-5-nitroaniline	0.5	0.7	-1.1	-1.2	-0.6	0.6	-1.0	-1.2

**Table S17.** Residual values calculated against the individual solid and all three solids QSARs, developed with data from this study. QSAR linear regressions provided in **Table S11**.

	Simple substituents				All substituents			
	$\Sigma\sigma$	pK <sub>a</sub>	E <sub>HOMO</sub>	E <sub>ox,corr.</sub>	$\Sigma\sigma$	pK <sub>a</sub>	E <sub>HOMO</sub>	E <sub>ox,corr.</sub>
<i>Drinking water treatment solids</i>								
phenol	-0.5	-0.7	-0.1	-0.4	-0.3	-0.5	-0.06	-0.3
resorcinol	0.4	0.2	0.3	0.05	0.5	0.3	0.4	0.2
estrone		-0.1				0.1		
4-cresol	0.09	-0.01	0.3	-0.2	0.2	0.2	0.5	0.09
4- <i>tert</i> -octylphenol	0.9	0.7			1.0	0.9		
bisphenol A		0.1	-0.04	1.1		0.3	0.3	1.1
4-phenoxyphenol		1.6	1.9	0.8		1.7	2.0	1.1
4-nitrocatechol		2.0	1.8	1.7		1.8	1.7	1.8
triclosan		0.7	0.2	0.5		0.6	0.3	0.6
2-chlorophenol	-0.04	-0.7	-0.8	-1.1	-0.01	-0.8	-0.7	-0.9
3-chlorophenol	-0.6	-1.0	-0.8	-0.4	-0.5	-1.0	-0.7	-0.4
4-chlorophenol	-0.05	-0.3	-0.3	-0.7	0.04	-0.2	-0.2	-0.5
2-nitrophenol	0.5	-0.7	-0.7	-0.5	0.4	-0.9	-0.9	-0.6
3-nitrophenol	-0.4	-1.3	-0.7	-0.5	-0.3	-1.3	-0.8	-0.6
4,4'-dihydroxybiphenyl	-0.3	-0.4	-1.0	-0.5	-0.2	-0.3	-0.6	-0.3
<i>Acid mine drainage solids</i>								
phenol	0.4	0.3	0.7	0.5	0.7	0.6	1.0	0.8
resorcinol	0.4	0.5	0.4	0.3	0.8	0.6	0.7	0.5
estrone		-0.5				-0.2		
4-cresol	-0.4	-0.3	-0.1	-0.4	-0.07	-0.07	0.2	-0.2
4- <i>tert</i> -octylphenol	0.4	0.4			0.8	0.7		
bisphenol A		-0.3	-0.4	0.3		-0.08	-0.1	0.7
4-phenoxyphenol		0.7	0.8	0.1		0.9	1.2	0.2
4-nitrocatechol		2.7	2.1	2.2		2.6	2.5	2.5
triclosan		1.0	0.3	0.6		0.9	0.6	0.9
2-chlorophenol	-0.1	-0.6	-0.9	-1.1	0.2	-0.6	-0.6	-0.8
3-chlorophenol	-0.5	-0.7	-0.8	-0.6	-0.2	-0.7	-0.5	-0.1
4-chlorophenol	-0.3	-0.3	-0.5	-0.7	0.04	-0.2	-0.2	-0.5
2-nitrophenol	0.2	-0.6	-1.2	-1.0	0.5	-0.8	-0.8	-0.5
3-nitrophenol								
4,4'-dihydroxybiphenyl	-0.05	0.02	-0.4	-0.08	0.3	0.2	-0.1	0.2

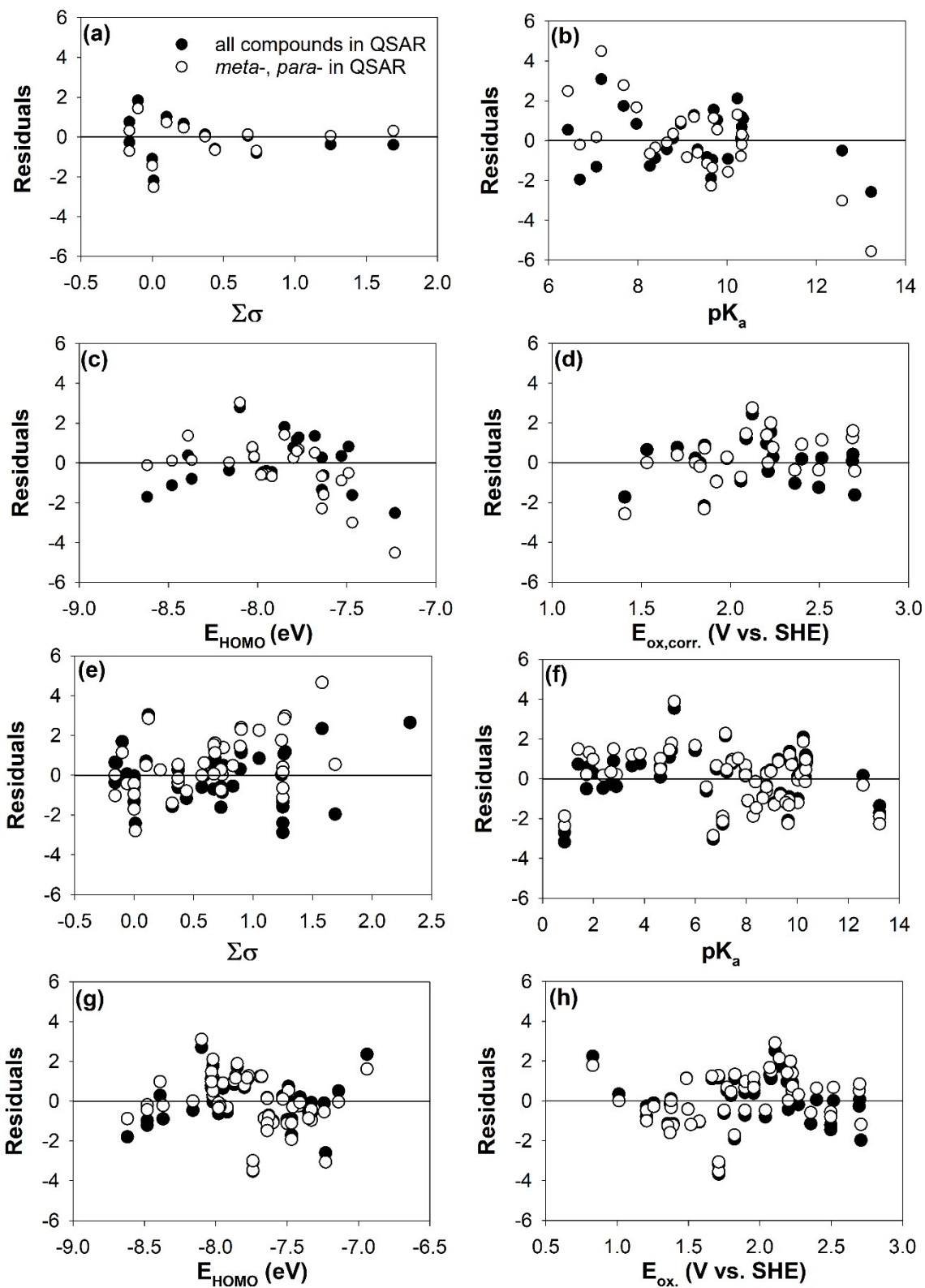


**Figure S9.** Plots of residuals versus independent QSAR descriptors for this study (a through d) and literature data (e through h). Residuals were calculated for QSAR relationships including either the simple (*meta*-, *para*-) or all compounds.

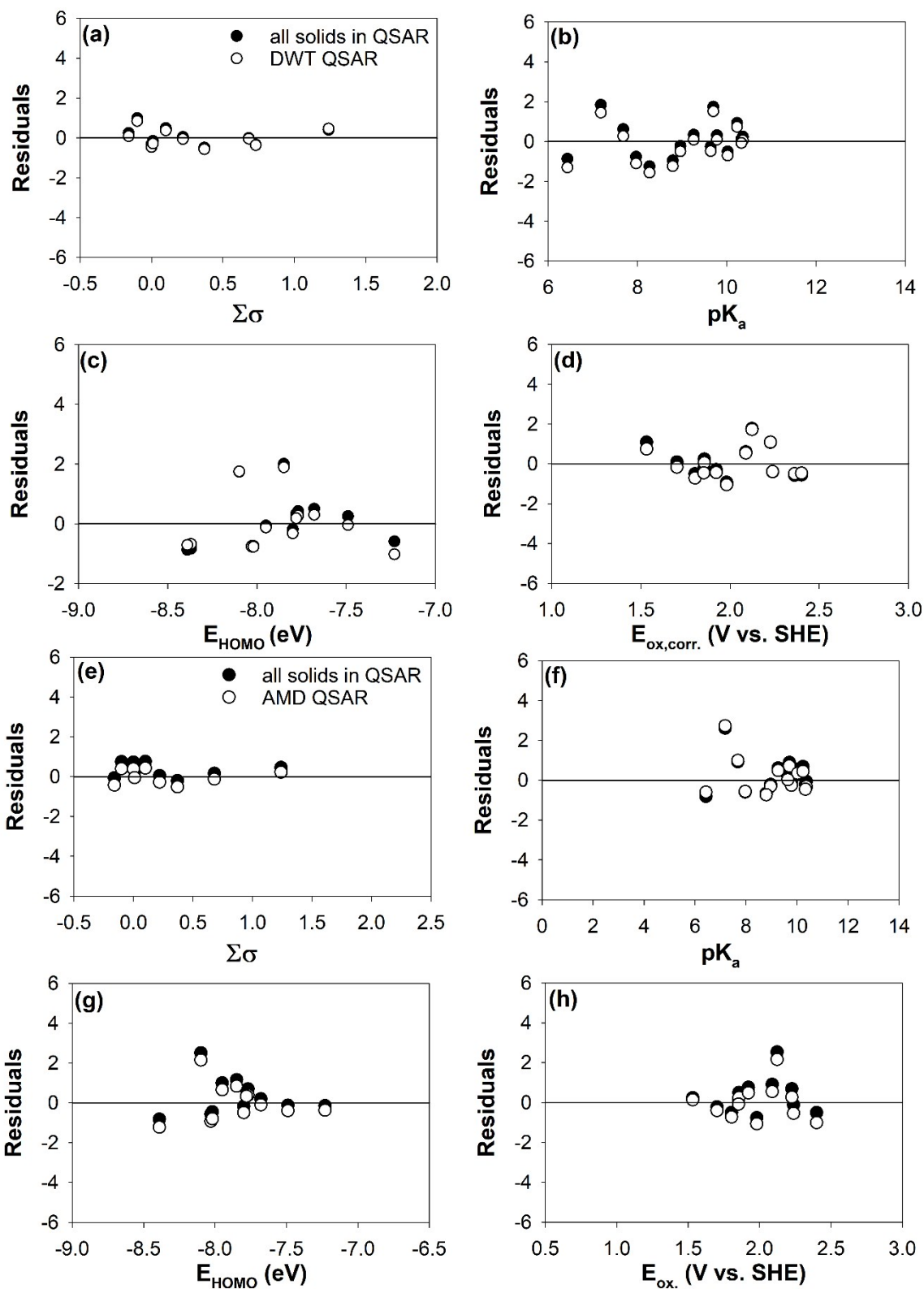


**Figure S10.** Plots of residuals versus independent QSAR descriptors for drinking water treatment (DWT) and acid mine drainage (AMD) solids. Residuals were calculated for QSAR relationships calculated for both the individual solids and all solids

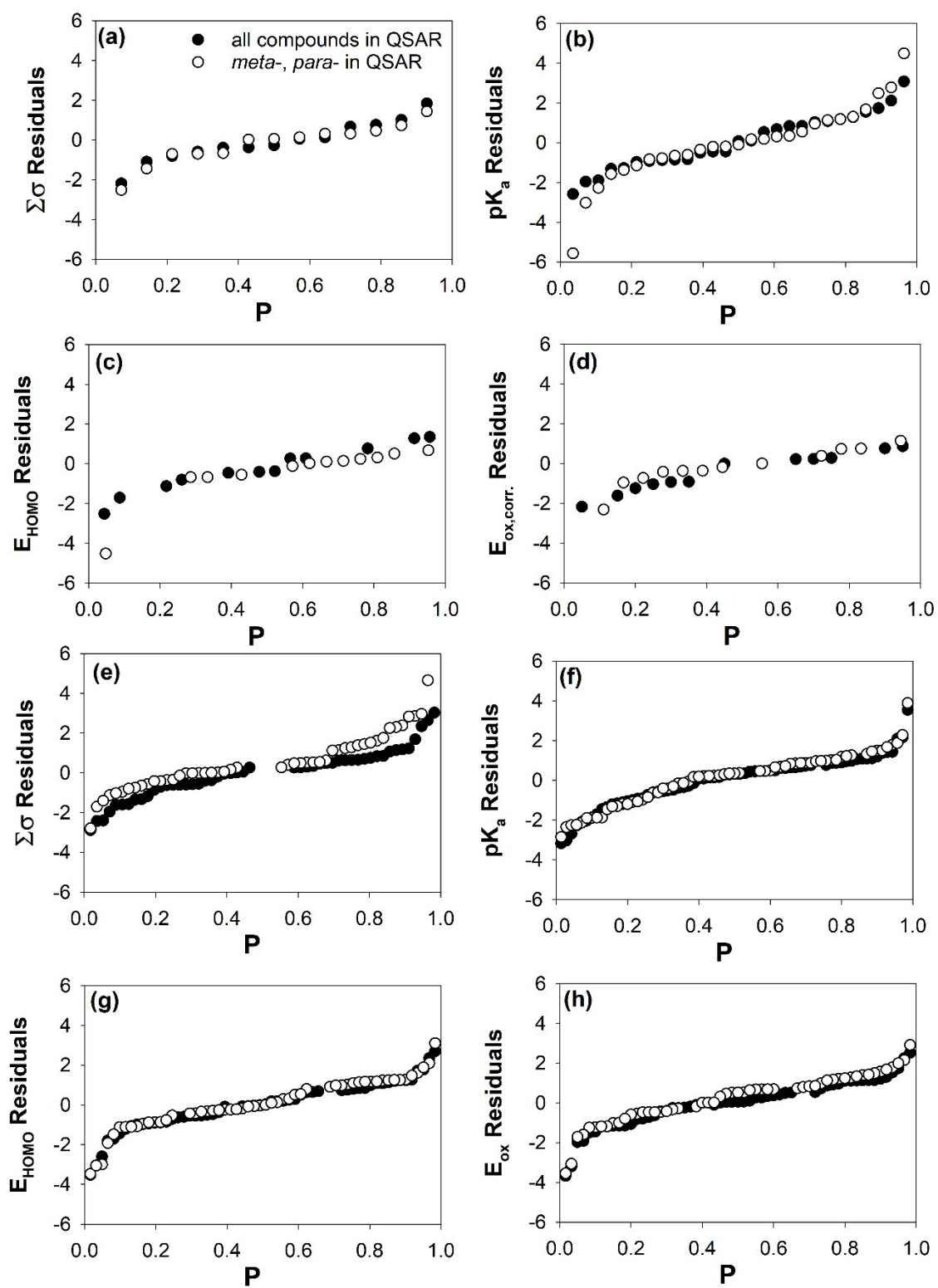


**Figure S11.** Residual normality plots of the calculated residuals versus probability (P) of each residual for QSAR relationships including using only simple *meta*- and *para*-substituted

compounds or all compounds. Plots (a) through (d) show data from only this study and plots (e) through (h) show the data for the larger literature data set.

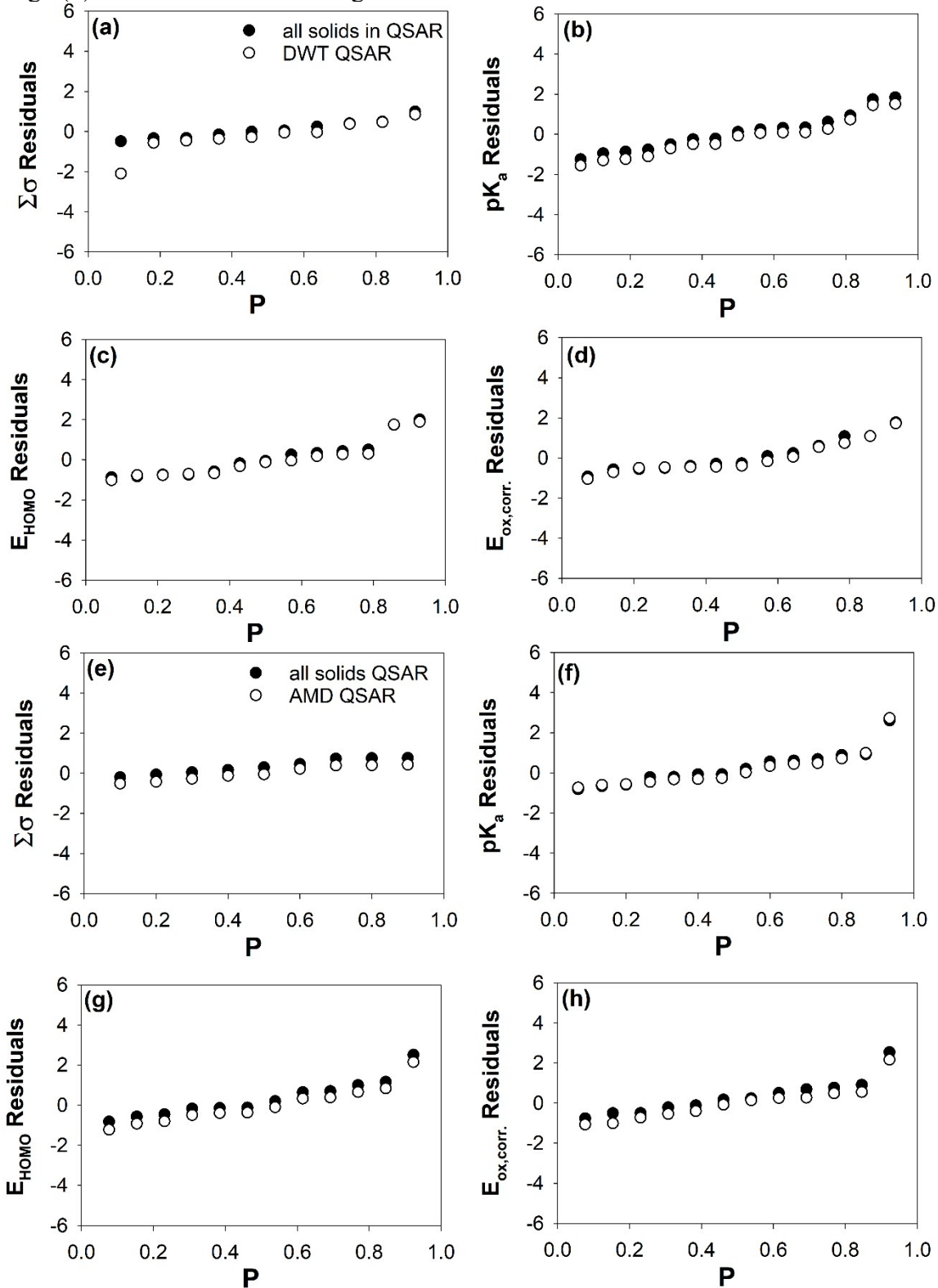


**Figure S12.** Residual normality plots of the calculated residuals versus probability of each residual for QSAR relationships including using only a single manganese oxide or all solids. Plots (a)

through (d) show data for drinking water treatment (DWT) solids and plots (e) through (h) show the data for the acid mine drainage (AMD) solids data.

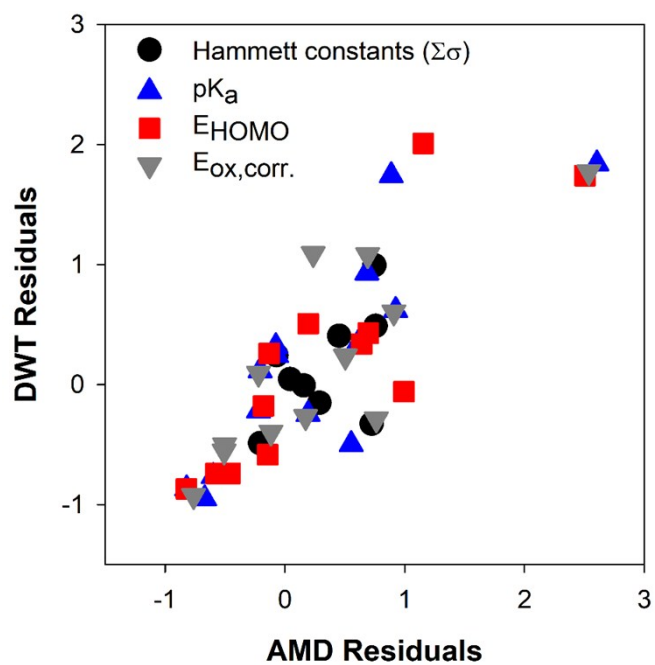


**Figure S13.** Residuals of each QSAR for phenols reacted with drinking water treatment solids (DWT) versus the residuals for phenols reacted with acid mine drainage solids (AMD).

**Table S18.** QSAR validation based on structural substitutions using data from this study with  $\delta$ -MnO<sub>2</sub> and literature. Gray values fall within the accepted ranges for that measure.

	Training	Test	Training set			Test set: Comparing predicted and experimental log ( $k/k_{4-Cl}$ ) values					
Accepted values	n	n	Slope	R <sup>2</sup>	p	r <sup>2</sup>	r <sub>m</sub> <sup>2</sup>	r <sub>m</sub> <sup>'2</sup>	R <sup>2</sup> <sub>pred</sub>	p	R <sup>2</sup> <sub>p</sub>
	-	-	-	> 0.6	< 0.05	-	> 0.5	> 0.5	> 0.5	< 0.05	> 0.5
<i>meta-, para-, ortho- training set, complex compounds test set</i>											
Hammett constant	53	2	1.43	0.21	0.001	1.00	0.06	0.03	0.54	-	0.07
pK <sub>a</sub>	55	14	0.18	0.09	0.01	0.03	0.01	0.02	0.28	0.58	0.03
E <sub>HOMO</sub>	48	12	1.48	0.10	0.03	0.02	-0.01	0.01	0.46	0.63	0.02
E <sub>ox</sub>	47	12	-1.19	0.08	0.20	0.07	-0.07	0.07	0.49	0.40	0.04
<i>meta-, para- training set, ortho- test set</i>											
Hammett constant	37	18	3.25	0.61	1.3E-8	0.37	0.08	0.29	-3.33	0.01	0.19
pK <sub>a</sub>	37	32	0.31	0.21	0.005	0.03	0.01	0.02	-0.01	0.34	0.03
E <sub>HOMO</sub>	34	26	2.11	0.17	0.01	0.06	-0.03	0.03	0.33	0.24	0.05
E <sub>ox</sub>	34	25	-1.61	0.14	0.03	0.01	-0.01	0.01	0.30	0.61	0.01
<i>meta-, para- training set, ortho-, complex test set</i>											
Hammett constant	37	16	3.25	0.61	1.3E-8	0.15	0.06	0.13	-3.66	0.15	0.14
pK <sub>a</sub>	37	18	0.31	0.21	0.005	0.02	-0.01	0.02	-0.22	0.54	0.02
E <sub>HOMO</sub>	34	14	2.11	0.17	0.01	0.09	-0.05	0.05	0.15	0.29	0.08
E <sub>ox</sub>	34	13	-1.61	0.14	0.03	0.10	-0.09	0.06	0.07	0.29	0.06
<i>Literature data training set This study test set</i>											
Hammett constant	39	16	-1.02	0.10	0.054	0.45	0.37	0.36	0.65	0.004	0.20
pK <sub>a</sub>	42	27	0.16	0.09	0.052	0.09	0.07	0.05	0.39	0.14	0.06
E <sub>HOMO</sub>	36	24	1.17	0.04	0.22	0.13	-0.08	0.12	0.62	0.08	0.10
E <sub>ox</sub>	36	23	-0.70	0.02	0.39	0.29	-0.48	0.19	0.36	0.008	0.23
	Training set	Test set	Training set			Test set: Comparing predicted and experimental log ( $k/k_{4-Cl}$ ) values					

Accepted values	n	n	Slope	R <sup>2</sup>	p	r <sup>2</sup>	r <sub>m</sub> <sup>2</sup>	r <sub>m</sub> <sup>'2</sup>	R <sup>2</sup> <sub>pred</sub>	p	R <sup>2</sup> <sub>p</sub>
	-	-	-	> 0.6	< 0.05	-	> 0.5	> 0.5	> 0.5	< 0.05	> 0.5
<i>This study training set</i>											
<i>Literature data test set</i>											
Hammett constant	16	39	-1.74	0.46	0.004	0.10	-0.02	0.09	0.25	0.054	0.08
pK <sub>a</sub>	27	42	0.26	0.09	0.04	0.09	-0.06	0.08	0.21	0.052	0.06
E <sub>HOMO</sub>	24	36	1.39	0.13	0.08	0.04	-0.01	0.04	0.37	0.22	0.03
E <sub>ox</sub>	23	36	-1.89	0.29	0.01	0.02	0.02	0.01	0.25	0.39	0.01
<i>Randomized training set</i>											
<i>Randomized test set</i>											
Hammett constant	39	16	-1.20	0.14	0.02	0.14	0.13	0.03	0.60	0.15	-
pK <sub>a</sub>	50	19	0.16	0.09	0.03	0.00	0.00	0.00	0.47	0.87	-
E <sub>HOMO</sub>	45	15	1.39	0.07	0.07	0.07	-0.02	0.06	0.57	0.34	-
E <sub>ox</sub>	45	14	-0.88	0.05	0.14	0.25	-0.19	0.19	0.61	0.07	-

**Table S19.** QSAR validation measures using data from this study with three manganese oxides (i.e.,  $\delta$ -MnO<sub>2</sub> and two reclaimed solids). Gray values fall within the accepted ranges for that measure.

	Training set	Test set	Training set			Test set: Comparing predicted and experimental log ( $k/k_{4Cl}$ ) values					
Accepted values	n	n	Slope	R <sup>2</sup>	p	r <sup>2</sup>	r <sub>m</sub> <sup>2</sup>	r <sub>m</sub> <sup>'2</sup>	r <sup>2</sup> <sub>pred</sub>	p	R <sup>2</sup> <sub>p</sub>
	-	-	-	> 0.6	< 0.05	-	> 0.5	> 0.5	> 0.5	< 0.05	> 0.5
<i><math>\delta</math>-MnO<sub>2</sub> training set, Reclaimed solids test set</i>											
Hammett constant	16	19	0.43	0.45	0.004	0.76	0.25	-0.09	0.36	1.0E-6	0.31
pK <sub>a</sub>	27	29	-0.35	0.06	0.22	0.12	0.06	-2.15	-0.02	0.07	0.09
E <sub>HOMO</sub>	24	25	-0.14	0.13	0.08	0.14	0.07	-0.15	-0.12	0.07	0.11
E <sub>ox</sub>	23	25	0.10	0.29	0.01	0.28	0.11	-0.09	0.23	0.01	0.22
<i>Randomized training set Randomized test set</i>											
Hammett constant	27	8	1.30	0.53	1.5E-5	0.41	0.28	0.20	0.32	0.09	-
pK <sub>a</sub>	38	18	-0.40	0.19	0.01	0.07	0.07	0.06	-0.70	0.28	-
E <sub>HOMO</sub>	34	15	0.62	0.13	0.04	0.08	0.07	0.01	0.05	0.31	-
E <sub>ox</sub>	33	15	0.61	0.38	1.5E-4	0.24	0.17	0.003	0.10	0.06	-

## References

- 1 J. W. Murray, The surface chemistry of hydrous manganese dioxide, *J. Colloid Interf. Sci.*, 1974, **46**, 357-371.
- 2 R. Hedin, T. Weaver, N. Wolfe and G. Watzlaf, presented in part at the 35th Annual National Association of Abandoned Mine Land Programs Conference, Daniels, West Virginia, 2013.
- 3 A. Manceau, M. A. Marcus and S. Grangeon, Determination of Mn valence states in mixed-valent manganates by XANES spectroscopy, *Am. Mineral.*, 2012, **97**, 816-827.
- 4 O. A. Ohlweiler and A. M. H. Schneider, Standardization of potassium permanganate by titration of sodium oxalate in presence of perchloric acid and manganese(II) sulfate, *Anal. Chim. Acta*, 1972, **58**, 477-480.
- 5 R. M. Fowler and H. A. Bright, Standardization of permanganate solutions with sodium oxalate, *J. Res. Natl. Bur. Stand.*, 1935, **15**, 493-501.
- 6 J. E. Post, Manganese oxide minerals: Crystal structures and economic and environmental significance, *Proc. Natl. Acad. Sci. U.S.A.*, 1999, **96**, 3447-3454.
- 7 C. K. Remucal and M. Ginder-Vogel, A critical review of the reactivity of manganese oxides with organic contaminants, *Environ. Sci. Process. Impacts*, 2014, **16**, 1247-1266.
- 8 A. T. Stone, Reductive dissolution of manganese(III/IV) oxides by substituted phenols, *Environ. Sci. Technol.*, 1987, **21**, 979-988.
- 9 H. J. Ulrich and A. T. Stone, Oxidation of chlorophenols adsorbed to manganese oxide surfaces, *Environ. Sci. Technol.*, 1989, **23**, 421-428.
- 10 S. Balgooyen, P. J. Alaimo, C. K. Remucal and M. Ginder-Vogel, Structural transformation of MnO<sub>2</sub> during the oxidation of bisphenol A, *Environ. Sci. Technol.*, 2017, **51**, 6053-6062.
- 11 S. Balgooyen, G. Campagnola, C. K. Remucal and M. Ginder-Vogel, Impact of bisphenol A influent concentration and reaction time on MnO<sub>2</sub> transformation in a stirred flow reactor, *Environ. Sci. Process. Impacts*, 2019, **21**, 19-27.
- 12 M. Villalobos, B. Toner, J. Bargar and G. Sposito, Characterization of the manganese oxide produced by *Pseudomonas putida* strain MnB1, *Geochim. Cosmochim. Acta*, 2003, **67**, 2649-2662.
- 13 E. E. Schulte and B. G. Hopkins, Estimation of organic matter by weight loss-on-ignition. 1996, SSSA Special Publication, **46**, 21-31.
- 14 M. Kosmulski, Isoelectric points and points of zero charge of metal (hydr)oxides: 50 years after Parks' review, *Adv. Colloid Interface Sci.*, 2016, **238**, 1-61.
- 15 T. Mahmood, M. T. Saddique, A. Naeem, P. Westerhoff, S. Mustafa and A. Alum, Comparison of different methods for the point of zero charge determination of NiO, *Ind. Eng. Chem. Res.*, 2011, **50**, 10017-10023.
- 16 J. Klausen, S. B. Haderlein and R. P. Schwarzenbach, Oxidation of substituted anilines by aqueous MnO<sub>2</sub>: Effect of co-solutes on initial and quasi-steady-state kinetics, *Environ. Sci. Technol.*, 1997, **31**, 2642-2649.
- 17 K. Rubert and J. A. Pedersen, Kinetics of oxytetracycline reaction with a hydrous manganese oxide, *Environ. Sci. Technol.*, 2006, **40**, 7216-7221.
- 18 S. C. Ying, B. D. Kocar, S. D. Griffis and S. Fendorf, Competitive microbially and Mn oxide mediated redox processes controlling arsenic speciation and partitioning, *Environ. Sci. Technol.*, 2011, **45**, 5572-5579.

- 19 W. S. Yao and F. J. Millero, Adsorption of phosphate on manganese dioxide in seawater, *Environ. Sci. Technol.*, 1996, **30**, 536-541.
- 20 Z. Moldovan, D. E. Popa, I. G. David, M. Buleandra and I. A. Badea, A derivative spectrometric method for hydroquinone determination in the presence of kojic acid, glycolic acid, and ascorbic acid, *J. Spectrosc.*, 2017, **2017**, 1-9.
- 21 A. T. Stone and J. J. Morgan, Reduction and dissolution of manganese(III) and manganese(IV) oxides by organics. 1. Reaction with hydroquinone, *Environ. Sci. Technol.*, 1984, **18**, 450-456.
- 22 H. Zhang, W. R. Chen and C. H. Huang, Kinetic modeling of oxidation of antibacterial agents by manganese oxide, *Environ. Sci. Technol.*, 2008, **42**, 5548-5554.
- 23 A. T. Stone and J. J. Morgan, Reduction and dissolution of manganese(III) and manganese(IV) oxides by organics: 2. Survey of the reactivity of organics, *Environ. Sci. Technol.*, 1984, **18**, 617-624.
- 24 N. Shaikh, H. Zhang, K. Rasamani, K. Artyushkova, A. S. Ali and J. M. Cerrato, Reaction of bisphenol A with synthetic and commercial  $MnO_{x(s)}$ : Spectroscopic and kinetic study, *Environ. Sci. Process. Impacts*, 2018, **20**, 1046-1055.
- 25 S. Canonica and P. G. Tratnyek, Quantitative structure-activity relationships for oxidation reactions of organic chemicals in water, *Environ. Toxicol. Chem.*, 2003, **22**, 1743-1754.
- 26 A. S. Pavitt, E. J. Bylaska and P. G. Tratnyek, Oxidation potentials of phenols and anilines: Correlation analysis of electrochemical and theoretical values, *Environ. Sci. Process. Impacts*, 2017, **19**, 339-349.
- 27 A. J. Salter-Blanc, E. J. Bylaska, M. A. Lyon, S. C. Ness and P. G. Tratnyek, Structure-activity relationships for rates of aromatic amine oxidation by manganese dioxide, *Environ. Sci. Technol.*, 2016, **50**, 5094-5102.
- 28 P. G. Tratnyek, E. J. Bylaska and E. J. Weber, In silico environmental chemical science: Properties and processes from statistical and computational modelling, *Environ. Sci. Process. Impacts*, 2017, **19**, 188-202.
- 29 Y. Lee and U. von Gunten, Quantitative structure-activity relationships (QSARs) for the transformation of organic micropollutants during oxidative water treatment, *Water Res.*, 2012, **46**, 6177-6195.
- 30 W. A. Arnold, Y. Oueis, M. O'Connor, J. E. Rinaman, M. G. Taggart, R. E. McCarthy, K. A. Foster and D. E. Latch, QSARs for phenols and phenolates: Oxidation potential as a predictor of reaction rate constants with photochemically produced oxidants, *Environ. Sci. Process. Impacts*, 2017, **19**, 324-338.
- 31 J. C. Suatoni, R. E. Snyder and R. O. Clark, Voltammetric studies of phenol and aniline ring substitution, *Anal. Chem.*, 1961, **33**, 1894-1897.
- 32 S. Laha and R. G. Luthy, Oxidation of aniline and other primary aromatic amines by manganese dioxide, *Environ. Sci. Technol.*, 1990, **24**, 363-373.
- 33 J. W. Park, J. Dec, J. E. Kim and J. M. Bollag, Effect of humic constituents on the transformation of chlorinated phenols and anilines in the presence of oxidoreductive enzymes or birnessite, *Environ. Sci. Technol.*, 1999, **33**, 2028-2034.
- 34 G. B. Barlin and D. D. Perrin, Prediction of the strengths of organic acids, *Q. Rev., Chem. Soc.*, 1966, 75-101.
- 35 J. Clark and D. D. Perrin, Prediction of the strengths of organic bases, *Q. Rev. Chem. Soc.*, 1964, 295-320.

- 36 C. Hansch, A. Leo and R. W. Taft, A survey of hammett substituent constants and resonance and field parameters, *Chem. Review*, 1991, **91**, 165-195.
- 37 M. Swain, Chemicalize.Org, *J. Chem. Inf. Model.*, 2012, **52**, 613-615.
- 38 M. Valiev, E. J. Bylaska, N. Govind, K. Kowalski, T. P. Straatsma, H. J. J. Van Dam, D. Wang, J. Nieplocha, E. Apra, T. L. Windus and W. de Jong, Nwchem: A comprehensive and scalable open-source solution for large scale molecular simulations, *Comput. Phys. Commun.*, 2010, **181**, 1477-1489.
- 39 U. EPA, Estimation programs interface suite™ for microsoft® windows. 2012.
- 40 J. L. Devore, *Probability & statistics for engineering and the sciences*, Brooks/Cole, Boston, MA, 8 edn., 2012.
- 41 P. G. Tratnyek, E. J. Weber and R. P. Schwarzenbach, Quantitative structure-activity relationships for chemical reductions of organic contaminants, *Environ. Toxicol. Chem.*, 2003, **22**, 1733-1742.
- 42 N. Frimayanti, M. L. Yam, H. B. Lee, R. Othman, S. M. Zain and N. A. Rahman, Validation of quantitative structure-activity relationship (QSAR) model for photosensitizer activity prediction, *Int. J. Mol. Sci.*, 2011, **12**, 8626-8644.
- 43 P. Gramatica, On the development and validation of QSAR models, *Methods Mol. Biol.*, 2013, **930**, 499-526.
- 44 R. Veerasamy, H. Rajak, A. Jain, S. Sivadasan, C. P. Varghese and R. K. Agrawal, Validation of QSAR models - strategies and importance, *Int. J. Drug Design Discov.*, 2011, **2**, 511-519.
- 45 A. Cherkasov, E. N. Muratov, D. Fourches, A. Varnek, Baskin, II, M. Cronin, J. Dearden, P. Gramatica, Y. C. Martin, R. Todeschini, V. Consonni, V. E. Kuz'min, R. Cramer, R. Benigni, C. Yang, J. Rathman, L. Terfloth, J. Gasteiger, A. Richard and A. Tropsha, QSAR modeling: Where have you been? Where are you going to?, *J. Med. Chem.*, 2014, **57**, 4977-5010.